**Table XI:** Characteristics of Metoramic Sciences binders and modifiers.

| Binders | | |
|---|---|---|
| Name | K565-4 | B-73305 |
| Resin Type | Acrylic | Vinyl |
| Solvents | Isopropyl alcohol<br>Heptane | Toluene<br>Ethyl alcohol |
| Solids | 24.89% (% of residue) | 22.3% |
| Viscosity | 60 cps | 550 cps |
| Specific Gravity of residue | 1.0 | 1.0 |
| Specific Gravity of binder | 0.79 | 0.88 |

| Modifiers: | | |
|---|---|---|
| Name: | M-1111 | M-1114 |
| Used when casting on: | glass/plastics | steels |
| Percentages to add to slurry: | 0.1-1% | 0.05-1% |

**Table XII:** Ceramic Tape Casting

| # | Ceramic | Vol% ceramic | Binder | Modifier | Results |
|---|---|---|---|---|---|
| 1 | SN-R (C) | 50.0 | Vinyl | M-1114 | Would not flow despite sonication |
| 2 | SN-R (C) | 48.3 | Vinyl | M-1114 | Additional solvent; cracked upon drying |
| 3 | SC-P (B) | 11.0 | Acrylic | M-1111 | Cast well; pliable tapes |
| 4 | SC-P (B) | 50.0 | Acrylic | M-1111 | Did not cast well; cracked upon drying |
| 5 | SC-P (B) | 30.0 | Acrylic | M-1111 | Not homogen ous; cracking |
| 6 | SC-P (B) | 40.0 | Acrylic | M-1111 | Cracked on drying |

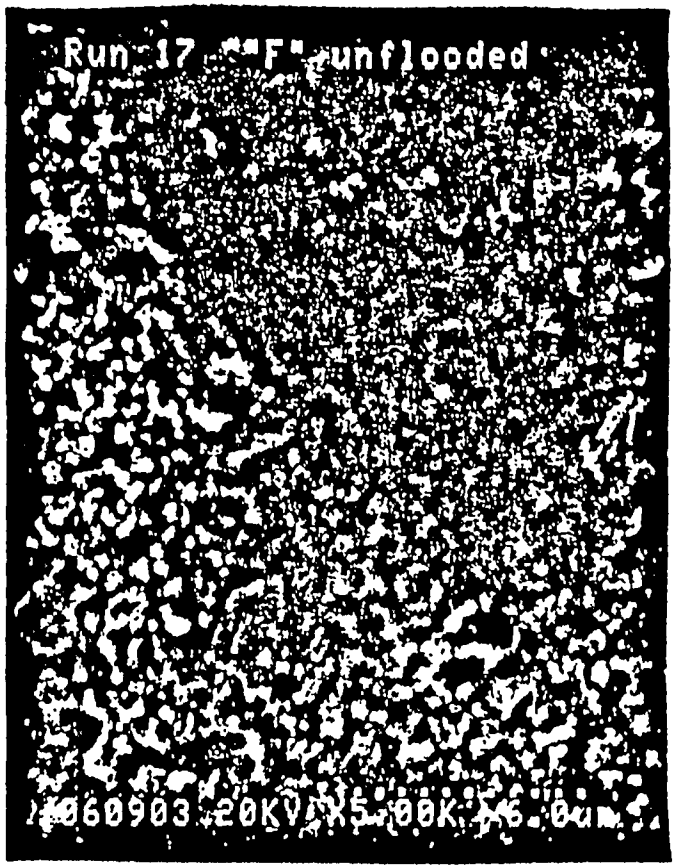


**Figure 53:** Pressed, tape cast F, showing an ordering of the surface over the unpressed tape.

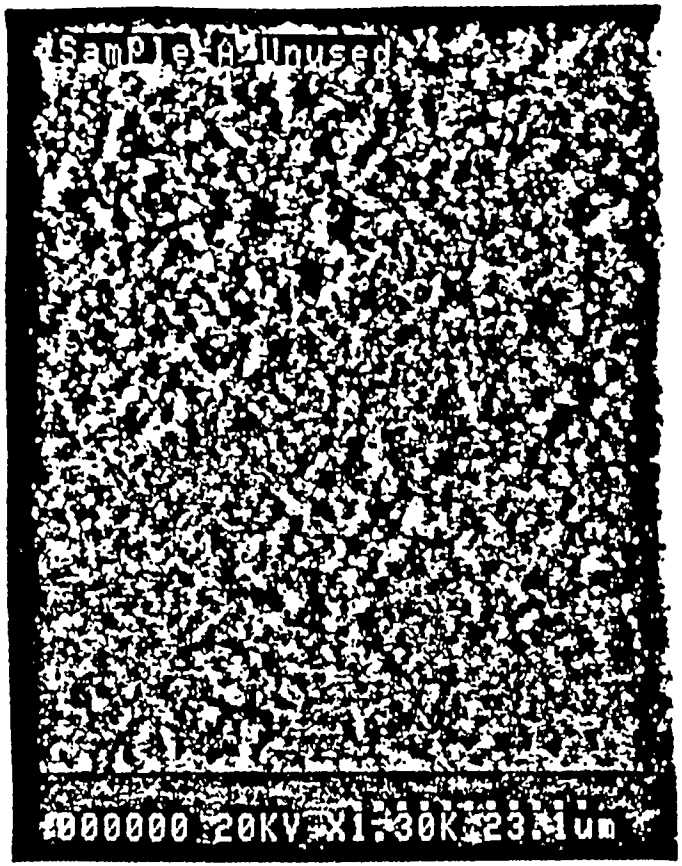


**Figure 54: 10-90 amorphous $SiO_2$ micrograph.**

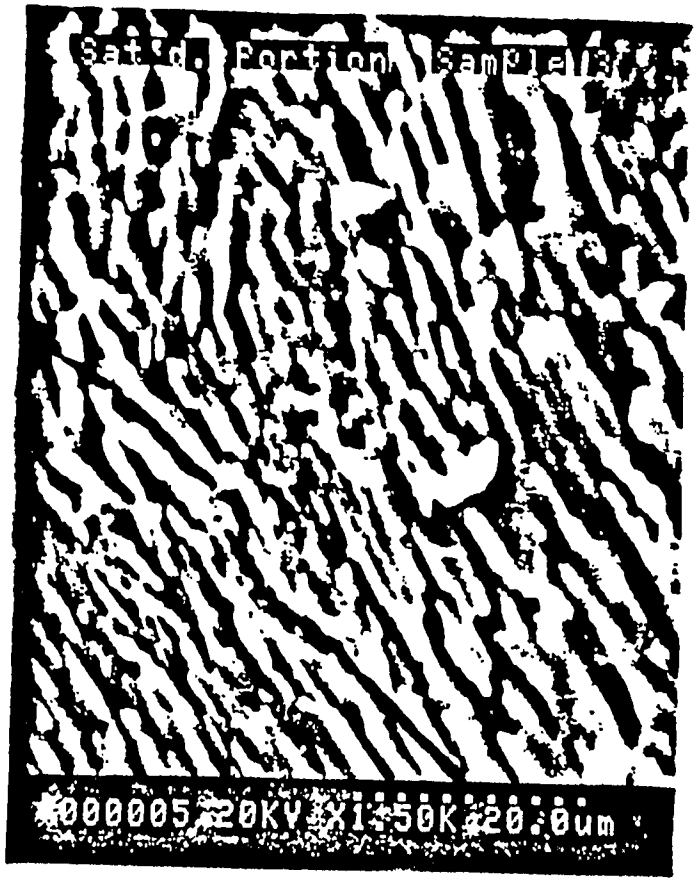


**Figure 55:** Micrograph of 10-90 amorphous $SiO_2$ saturated with electrolyte.

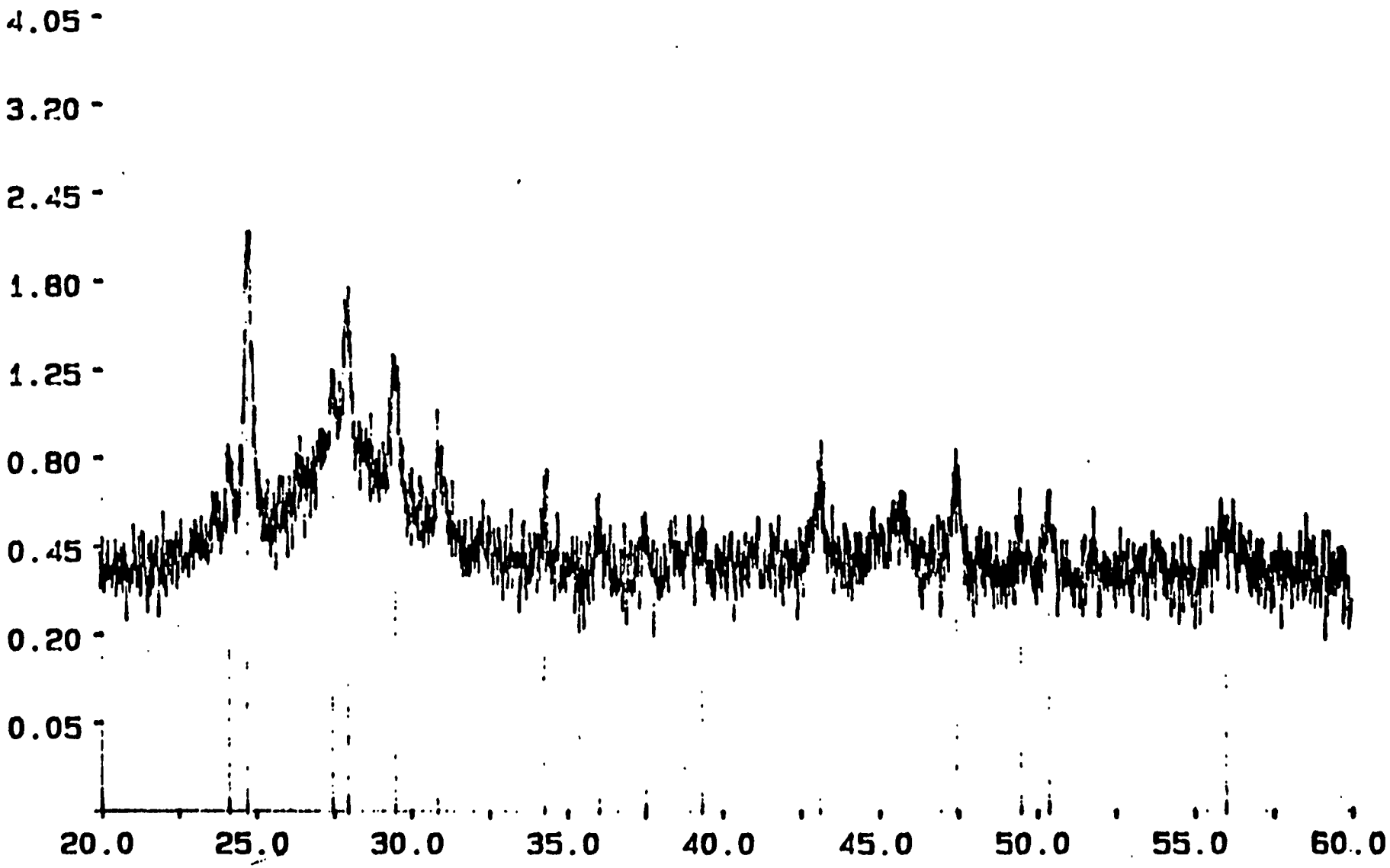


Figure 56: X-ray result of $SiO_2$ sol gel membrane after chemical testing.

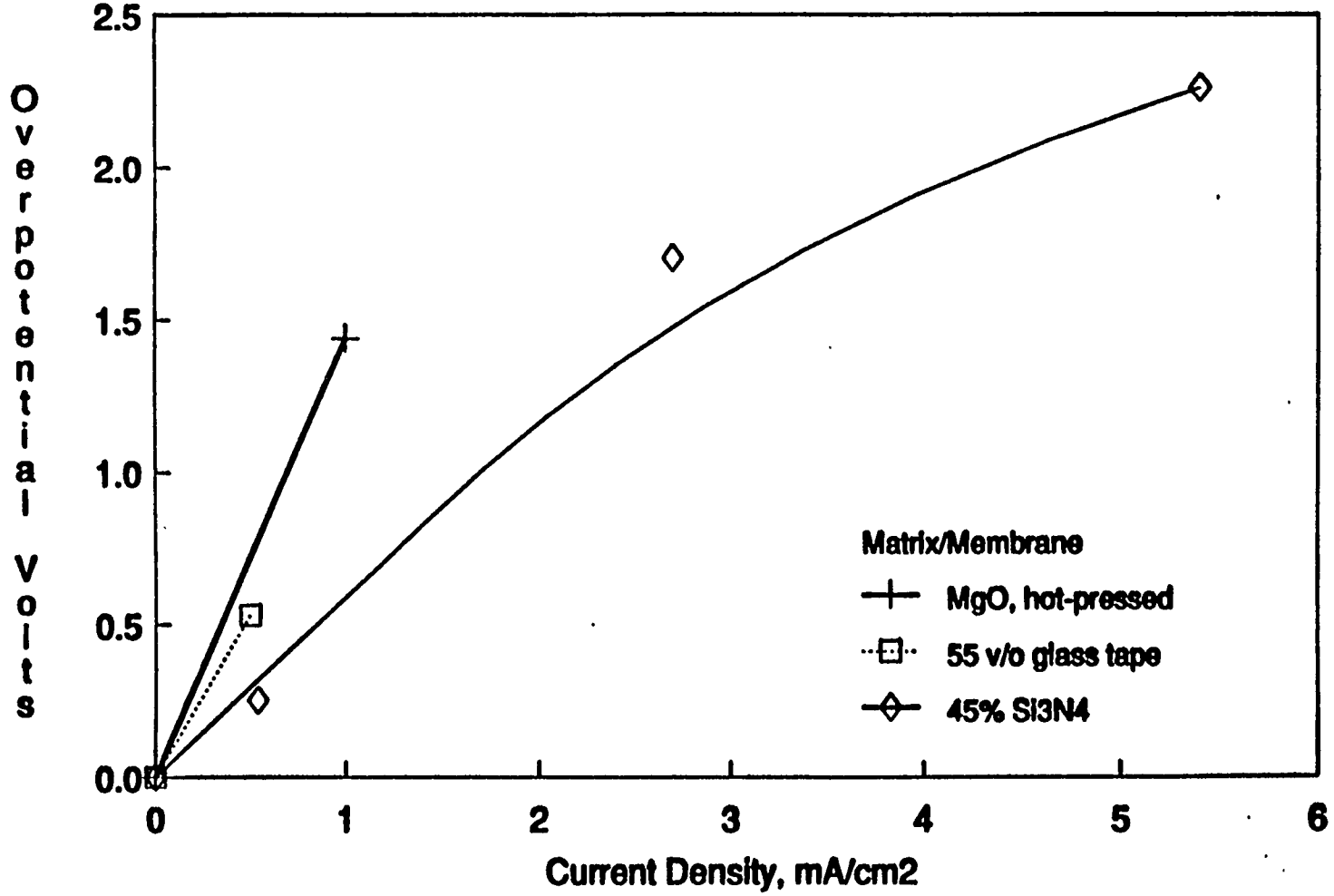


Figure 57: Cathodic polarization performance of different matrix materials using lithiated NiO electrodes.


**Figure 58:** $Si_3N_4$ sintered on alumina in air environment.

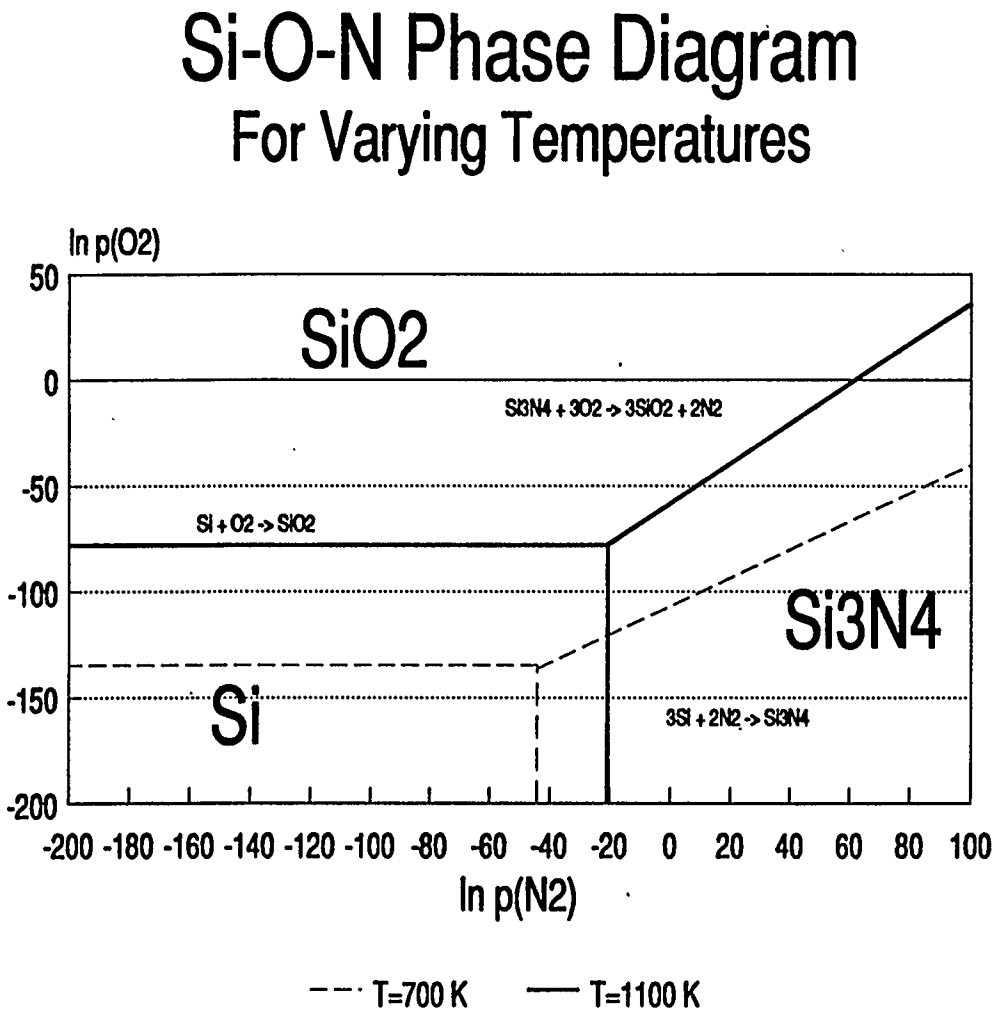


**Figure 59:** Silicon-oxygen-nitrogen phase diagram for the sintering of silicon at varying temperatures.

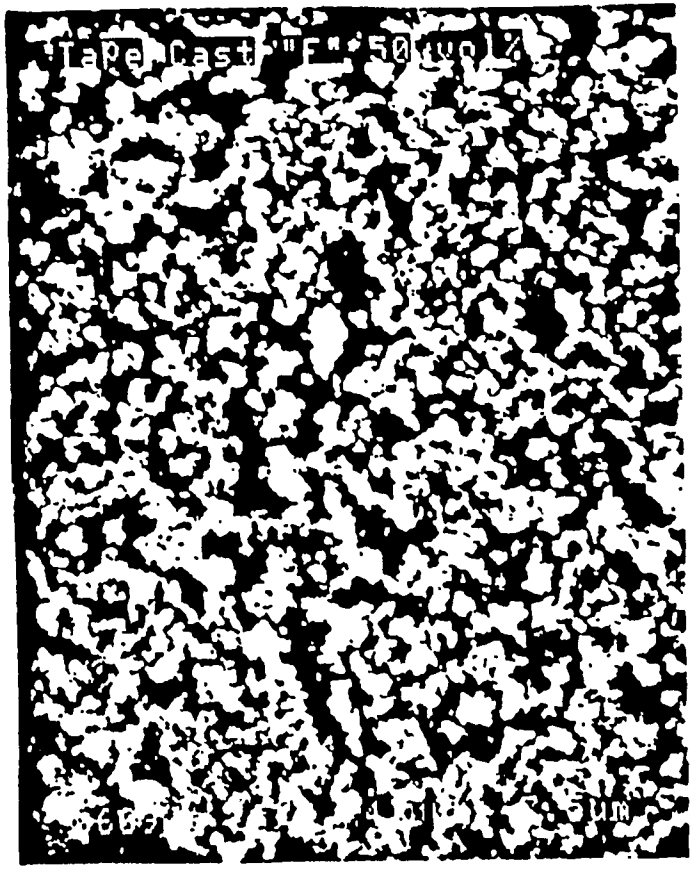




**Figure 60:** Tape cast F, unpressed, after binder burnout. 50 vol% loading.

FULL CELL TESTING

A laminated two-tape membrane was tested with lithiated NiO electrodes, achieving higher current densities and good polarization. The cell still produced quality data after 28 days on-line, compared to very early experiments which produced quality data for only three or four days. Most of this endurance came from the use of chemically stable electrode and matrix materials.

This configuration was very efficient at removing $SO_3$, showing visible decreases in the cathode exit plume three minutes after current was applied. A net generation of $SO_3$ at the anode was also detected within the first several minutes. Removal of 72% of inlet $SO_x$ was achieved with current equal to 90% removal (50 mA). The residual $SO_x$ detected in the outlet stream was partially in the form of $SO_2$, coming from the electrochemical reduction of $K_2S_2O_7$ (1). At low current densities, this generation was not a

$$S_2O_7^{2-} + 2e^- \rightarrow 3SO_4^{2-} + SO_2 \qquad (61)$$

problem, but as current densities exceeded 1.0 mA/cm$^2$, $SO_2$ generation became detectable. As the current density is increased, the gas flow increases in a linear fashion, sweeping the generated $SO_2$ away from the electrode surface.

The $SO_2$ generation was seen to increase with increasing current. At 50 mA, with 90% removal current equal to 100 mA, $SO_x$ removal was 72%. The removal was in excess of 45% because of residual removal (30%) at open circuit. This phenomena always occurs if the electrolyte contains excess sulfate. When the current was doubled to that equal to

90% removal, removal dropped to 56%. During this run, $SO_3$ was barely visible in the cathode outlet stream at 100 mA, confirming the presence of higher levels of $SO_2$ in the effluent.

At 5 mA/cm$^2$, the incoming gas stream (275 ml/min, 36 cm/sec superficial velocity) did not remain in the inlet tubes long enough to provide adequate heating. The gas then enters the Pt pre-oxidation catalyst bed below 400° C, kinetically preventing equilibrium conversion to $SO_3$ (99% $SO_3$). Also, since the gas enters the cell cold, it chills the surface of the electrode, causing partial freezing of the $SO_4^{2-}$ enriched catholyte, increasing the polarization at the cathode. The oxidation of the inlet $SO_2$ was solved by installing an auxiliary reactor, towards the end of this run, to convert the $SO_2$ to $SO_3$ before entering the cell. This did not solve the problem of $SO_2$ generation, because the gas partially cooled between the auxiliary reactor and the cell entrance. A modified cell design, allowing longer residence time in the heated tubes, should stop this problem.

After the auxiliary reactor was installed, several applied current experiments were applied. Although the results exhibited the same general trend of $SO_2$ generation with increasing current, removals were several percentage points higher using the auxiliary reactor, but not outside the range of experimental error. $SO_2$ generation was quantified via gas chromatography, and showed that above 20 mA current, $SO_2$ was present in the cathode outlet stream, at a level of ~13% of inlet concentration.

Currents as high as 200 mA (10.8 mA/cm$^2$ at the cathode) were reached for 10 minutes (after 3 hours at 100 mA), but with unacceptable voltages (-4.4V at cathode, +9V at anode) due to the cool gas stream and low $SO_2$ oxidation mentioned above.

Only minor degradation in performance was detected throughout the experiment. The electrolyte membrane did show some decay in performance, as measured by solution resistance and gas crossover. Many of the experiments were conducted at current levels above the system's ability to remove $SO_x$, due to the previously mentioned limitations. This had the effect of a net consumption of electrolyte through the electrochemical reactions at both the cathode and anode. The cathodic reaction (62) can

$$S_2O_7^{2-} + 2e^- \rightarrow 3SO_4^{2-} + SO_2 \qquad (62)$$

result in a net loss if the generated $SO_2$ is not oxidized, as seen in this experiment. The anodic reaction (63) can also consume electrolyte, since it proceeds unimpeded. After

$$SO_4^{2-} \rightarrow SO_3 + \frac{1}{2}O_2 + 2e^- \qquad (63)$$

running above removal limitations, the membrane is "dried", increasing resistance and eventually allowing gas crossover.

When gas crossover was seen, additional electrolyte was added, with the effect of stopping crossover, but with no effect on polarization. In a cell with high surface area enhancement electrodes, excess electrolyte has the effect of flooding electrode pores and increasing polarization. Because the present electrodes have a low enhancement factor (12x), excess electrolyte did not cause pore flooding. Any excess that could not be held in the membrane ran out the sides of the cell.

Overpotential behavior for all runs was very reproducible. Figure 61 demonstrates the reproducibility of the data, with only a minor shift in the initial anodic behavior between runs. The cathodic drift to more negative potentials over time shows a gradual

accumulation of $SO_4^{2-}$ on the electrode, due to the less than theoretical removals (described earlier).

A standard polarization curve of overpotential versus applied current density is shown in Figure 62 for the present cell in comparison with previous cells. Note that the present configuration, with 45% $Si_3N_4$ and no flooding, shows substantial improvement in polarization performance over the other membranes. Five times as much current was passed with only a 50% increase in overvoltage driving force. This shows that the proper selection of matrix material and processing conditions can result in substantial performance increases, even with the above mentioned problems.

Another successful run was conducted with Fibrex electrodes and two 42 vol. % ceramic tapes laminated together. Superb seals were formed between the membrane and housings, but a decrease in sealing ability was noticed as the run progressed. Removal was quite high (>90%) and equivalent to stoichiometry, within the bounds of experimental error.

With applied current equal to 90% stoichiometric removal, cathodic removal of $SO_3$ reached 90% or greater, given adequate time. Several levels of $V_2O_5$ electrolyte loading were used, for reasons explained below. Figure 63 shows removal data after ten minutes of applied current. The data point at 12.5 mA/cm$^2$ was obtained by following a different current path (5 mA/cm$^2$ = 36% removal for 2 hrs. then 10 mA/cm$^2$ = 72% removal for 2 hrs.) which generated the required sulfate ions for high $SO_3$ removal. Figure 64 shows removal data for the same runs, but after one hour. Removal is seen to be near 90%, in accordance with stoichiometry, for most currents, within the bounds of

experimental error. Removal in excess of stoichiometry may be due to reaction with sulfate ions which have accumulated since current was applied, during the periods of lower removal, but is not outside the experimental error.

Looking at removal rates for 690 cc/min of cathode gas, excess removal above the stoichiometric level is seen for all applied currents in Figure 65 This is due to residual and excess sulfate in the electrolyte which is quickly neutralized by any $SO_3$ present in the gas phase. The excess sulfate is caused by the generation of $SO_2$ at the cathode (described next). Residual sulfate in the electrolyte from previous runs produces removal at zero current.

With the present configuration, a new phenomenon was observed. As current was applied, $SO_2$ was seen to exit the cathode, Figure 66. This is possible from the electrochemistry of the system as seen by Scott[42] in free-electrolyte, but had not been observed before in high surface area (perovskite) electrode full cell tests. As current rises, $SO_2$ is generated at a faster rate, one which overcomes the rate of oxidation by $V_2O_5$ in the electrolyte. It appears that $SO_2$ is diffusing out of the porous cathode before it can contact sufficient $V_2O_5$ and is carried off by the passing gas stream. Calculations of outlet flow rates showed that one-half of the generated $SO_2$ is being oxidized by the $V_2O_5$ and removed at the cathode, for a 5 wt% $V_2O_5$ electrolyte. To overcome this problem, more $V_2O_5$ in $K_2S_2O_7$ was added to the cell through the reference port. At 7 wt.% $V_2O_5$ in the electrolyte, three-quarters of electrochemically generated $SO_2$ was oxidized and removed, Figure 67.

At 10 wt.% $V_2O_5$, approximately 5/8 of generated $SO_2$ was oxidized and removed according to calculation of the slope of the line through the data with applied current (Figure 68). This rate of oxidation is less than that for the 7 wt.% $V_2O_5$ study, but two major differences were present: First, flow was continuously provided at a level such that 90% stoichiometric removal would occur at 12.5 $mA/cm^2$, so that $SO_2$ which escapes the electrolyte at lower current densities does not have sufficient residence time to diffuse back to the electrolyte. Second, $SO_2$ was present at zero current, showing that the pre-oxidation catalyst was not saturated with an equilibrium level of $SO_2$ at the start of the run. Post-mortem analysis will confirm actual $V_2O_5$ loading.

At the anode, $SO_3$ generation is seen to deviate from stoichiometry at all $V_2O_5$ levels, Figure 69 and Figure 70. This discrepancy can be explained by two causes. The first, gas leakage out of the wet seal, accounts for most of the discrepancy at the higher $V_2O_5$ and current levels. The second cause is attributed to residual sulfate ions accumulating at the anode, as seen by cathodic $SO_2$ generation data. When $SO_2$ is generated at the cathode and not oxidized and removed, excess sulfate ions accumulate in the electrolyte and migrate to the anode under the influence of the applied electrical potential. Sulfate is either oxidized or raises the melting point of the electrolyte to the point where the electrolyte freezes on the anode surfaces. Excess sulfate at the anode will absorb electrochemically generated $SO_3$ and neutralize it to form the $S_2O_7^{2-}$ ion. This second phenomenon is confirmed by polarization data.

The effect of increasing $V_2O_5$ content is minimal after this short duration. After one hour of applied current (Figure 71), a greater effect of $V_2O_5$ loading is observed. As

$V_2O_5$ content increases, polarization decreases. The anodic polarization suffers from sulfate accumulation at the lower $V_2O_5$ loadings. This finding proves that increased vanadia loadings oxidize more of the cathodically-generated $SO_2$ before it can escape from the electrolyte.

Also, as each current application progressed, the anodic overpotential and electrical resistance were seen to increase with time. This phenomenon confirms that accumulated sulfate migrates to the anode, where it raises the melting point of the electrolyte and retards the anodic electrochemical reaction. The increase in resistance shows that the sulfate is building up in the area of the electrical contact.

Electrochemical kinetic data can be obtained by properly treating the overpotential data. The Butler-Volmer equation of electrochemical kinetics,

$$i = i_0[e^{(1-\alpha)\eta F/RT} - e^{-\alpha\eta F/RT}] \qquad (64)$$

can be applied at low overpotentials in the linearized form of

to determine $i_0$, the exchange current density. The other parameters are R, the gas constant, n, the number of electrons involved in the charge transfer reaction, and F,

$$i_0 = -\frac{RT}{nF}\left(\frac{di}{d\eta}\right) \qquad (65)$$

Faraday's constant. Data from the present run was reduced using equation (2) and is presented in Table XII, along with data from Franke[43], who used $La_{0.8}Sr_{0.2}CoO_3$ electrodes. These data show that the electrochemical kinetics at the cathode have

improved 50% under the same conditions of electrolyte composition and temperature (5%, 400° C), further substantiating the improved performance of the lithiated nickel oxide electrodes. With an increase in $V_2O_5$, the exchange current density has increased four times. While there is some improvement here, free electrolyte studies have shown the exchange current density to be 30 mA/cm$^2$ in $SO_3$-saturated electrolyte. The discrepancy here can be attributed to partial flooding of the electrode pores and diffusional resistances.

Another full cell test used a 49 volume percent silicon nitride tape cast matrix with 10 wt.% $V_2O_5$ in $K_2S_2O_7$ electrolyte, lithiated NiO electrodes and Macor housings with platinum leads. Some difficulty was encountered during start-up with insufficient electrolyte loading, but was corrected with electrolyte additions through the reference electrode port in the top housing. Also, an excessive pressure drop was detected through the pre-oxidation catalyst bed at high flow rates.

Operation with 50 or 100 mA did produce some $SO_2$ at the cathode outlet, a possibility from the electrochemical reduction of pyrosulfate:

$$2S_2O_7^{2-} + 2e^- \rightarrow 3SO_4^{2-} + SO_2 \qquad (66)$$

Generation of $SO_2$ was 11% at 50 mA and varied from 17% to 24% at 100 mA, relative to inlet flow rate. For $SO_3$, removal (relative to equilibrium conversion of inlet $SO_2$) at 50 mA was 89% and 80% to 83% at 100 mA for a flow rate equal to 90% stoichiometric removal. One of the electrodes was kept in a vacuum desiccator and later analyzed with Electron Surface Characterization Analysis (ESCA). Investigation of the resulting peaks

showed no Ni-S bonds present, negating the possibility of nickel sulfides or sulfates as corrosion products.

The increase in $SO_2$ generation is due to a combination of factors. First, $SO_2$ generation is directly proportional to applied current, but does not follow the same slope in Figure 72. Second, as current increases, so does the gas flow rate, which means any gas escaping the membrane has a lower residence time and therefore lower contact time with the $V_2O_5$ in the electrolyte, however, the slope again does not follow that of the stoichiometric curve in Figure 72. Third, $V^{5+}$ in the vanadium complex is reduced by $SO_2$ to $V^{4+}$, which has limited solubility in the melt. If this complex is not re-oxidized by gaseous oxygen, precipitation occurs, reducing the amount of catalyst available for $SO_2$ oxidation. This appears to be the case with the data.

Calculations of the rates of absorption of $SO_2$ and $O_2$ into vanadia-pyrosulfate melts and the re-oxidation of $V^{4+}$ were performed to see if the melt chemistry is limiting removal performance. The work of Holroyd and Kenney[44] for $SO_2$ absorption into films of molten $V_2O_5/K_2S_2O_7$ can be applied to the present process to show that the initial rate of absorption is $36 \times 10^{-9}$ gmol/cm$^2$/min. At 100 mA of current, $SO_2$ is electrochemically generated at the rate of $15.5 \times 10^{-6}$ gmol/min. Complete absorption, assuming total escape of generated $SO_2$, would require a melt surface area of 430 cm$^2$, or an electrode surface area enhancement of 21.5. These numbers increase linearly with increasing current. Holroyd and Kenney also investigated the reoxidation of $V^{4+}$ in the same melts[45] and found that $V^{4+}$ has a maximum solubility of 4% at 400° C. From their reaction constants, the rate of reoxidation in this system can be calculated as $14.5 \times 10^{-6}$ gmol/cm$^2$/min for

4% $V^{4+}$. With the rate of reoxidation being orders of magnitude faster than the absorption of $SO_2$, this step cannot be limiting.

However, Mars and Maessen[46] determined that there was a deviation from their normal kinetic behavior at lower temperatures (T < 415° C) for sulfuric acid catalyst pellets. They attributed this to either an increase in the rate-retarding effect of $SO_3$ or the formation of sulfovanadates, which would stabilize $V^{4+}$, reducing the rate of reoxidation. Both the rate of $SO_2$ absorption and the rate of reoxidation could be limiting and therefore an experiment will be conducted next quarter to determine the conversion of $SO_2$ to $SO_3$ bubbled through molten 10 wt.% $V_2O_5/K_2S_2O_7$.

Experimentation then focused on determination of the feasability of using commercial sulfuric acid catalyst (Haldor-Topsoe VK38) in the gas channels of the flow cell to convert the electrochemically generated $SO_2$ to $SO_3$ for removal. A tests was performed using thin cylinders of catalyst trimmed from 6 mm x 6mm catalyst pellets. This test showed a mass transfer limitation to the reaction rate (the horizontal asymptote in Figure 73) with a maximum rate of $10\times10^{-6}$ moles $SO_2$/min or $30\times10^{-6}$ moles $SO_2$/min/g catalyst at 400° C. At 375° C, this reaction was 5% slower, Figure 74.

Franke[47] shows the electrochemical reduction of the pyrosulfate as shown in Equation (66). This reaction must occur at the electrode/electrolyte interface due to the electron transfer required.

$$SO_2 + O_2 + 2e^- \rightarrow SO_4^{-2} \qquad (67)$$

$$2SO_2 + 2SO_4^{-2} \rightarrow 2S_2O_8^{-2} \quad (68)$$

$$SO_2 + O_2^{-2} \rightarrow SO_4^{-2} \quad (69)$$

$$E = E^o - \frac{RT}{nF}\ln\left(\frac{x_{SO_4^{-2}}\gamma_{SO_4^{-2}}}{P_{SO_2}P_{O_2}}\right) \quad (70)$$

The $SO_2$ then reacts with the superoxide ion according to Equation (69) and also with sulfate ions present. For the $SO_2$ to enter the gas stream, it must diffuse through the electrolyte, and into the gas stream. This mass transfer action is in direct opposition to the diffusion of $SO_3$ from the gas stream to the electrolyte where it reacts. ($SO_3$ dissolves in the electrolyte, and quickly reacts with the sulfate ion to form the pyrosulfate ion.) Should the superoxide ion not be present (due to the reduction of the vanadium pentoxide) in high enough concentration at the interface, the $SO_2$ can escape the cell, possibly the cause of the $SO_2$ production. The overall cathodic cell reaction can be written as seen in Equation (67). The Nerstian potential for this reaction can be written as in Equation (70), where the activity for the gaseous species is approximated as the partial pressure in atmospheres, and the activity of the solvated species is the mole fraction times the activity coefficient. $E^o$ is the standard reversible potential, and E is the equilibrium potential. It would be suspected that increasing the partial pressure would have the effect of pushing the equilibrium to the right, thus producing more sulfate ions, reducing the amount of $SO_2$ production. while lowering the equilibrium potential.

The anodic overall reaction can be written as in Equation (71), so an increase in

$$SO_4^{-2} \rightarrow SO_3 + \frac{1}{2}O_2 + 2e^- \qquad (71)$$

the dissolved $O_2$ would increase the reaction resistance unless the availability of the $SO_4^{-2}$ is relatively high.

Another possible explanation for the low removal is the removal of $O_2$ and $SO_2$ to form pyrosulfate through a complex of reactions utilizing complexes of vanadium

$$O_2 + 2[K_2\text{-}V_2O_4\text{-}3SO_3] \rightleftharpoons 2[K_2O\text{-}V_2O_5\text{-}2SO_3] + 2SO_3 \qquad (72)$$

$$[K_2O\text{-}V_2O_5\text{-}2SO_3] + 2SO_3 \rightleftharpoons [K_2O\text{-}V_2O_5\text{-}4SO_3] \qquad (73)$$

$$[K_2O\text{-}V_2O_5\text{-}4SO_3] + 2e^- \rightleftharpoons [K_2O\text{-}V_2O_4\text{-}3SO_3] + SO_4^{2-} \qquad (74)$$

$$2SO_3 + 2SO_4^{2-} \rightleftharpoons 2S_2O_7^{2-} \qquad (75)$$

pentoxide. The sum of the reactions contained in equations (72) through (75) is shown

$$O_2+SO_4^{2-}+2SO_3+2e^-+[K_2O\text{-}V_2O_4\text{-}3SO_3] \rightleftharpoons 2S_2O_7^{2-}+[K_2O\text{-}V_2O_5\text{-}2SO_3] \qquad (76)$$

in equation (76). The net result is the formation of pyrosulfate and a vanadium oxide complex through the utilization of oxygen, sulfate, and sulfur trioxide, and the use of two electrons. This mechanism is suggested by McHenry[48], and could explain the

apparent difference between the stoichiometric removal levels, and the actual removal levels.

The cell, again with pellets of VK38 in the flow channels, was run with the simulated flue gas over the cathode side of the cell at a 500 cc/min flowrate, and a pure $N_2$ sweep over the anode side of the cell. Removal data at this flow rate can be seen to be higher than that of stoichiometric removal rates in Figure 75. This may be due to the absorption of the gas into the cell in an attempt to reach a solubility equilibrium, to the presence of sulfates at the electrode surface, or to the method of mass flow evaluation.

As in the past, it was noticed that the polarity of the cell increased over time as seen in Figure 76, possibly due to the formation of a large, insoluble amount of sulfate at the surface of the electrode. The addition of 1g of electrolyte to the system decreased the polarity of the cell by approximately 65% at virtually constant stoichiometric removal rates. Should the reason for the increased cell polarity be the formation of a layer of sulfate, such a response would be expected, as the addition of the pyrosulfate/pentoxide mixture would tend to dissolve the sulfate formation, and place fresh pyrosulfate at the gas/molten salt/electrode interface. $SO_2$ production at the cathode was observed as the total applied current increased.

After taking a reading of the cell at 100 mA and a 500 cc/min flowrate, the partial pressure was doubled, and a measure of the $SO_2$ generation was taken. Figure 78 shows the extrapolated values obtained. It was not known, however, how much of this change in $SO_2$ generation was due to the electrochemistry of the cell, and how much was due to the oxidation (and possibly increase in activity) of the VK38 pellets in the channel. The

cell was then run for an additional 24 hours to determine the long term effects of doubling the $O_2$ partial pressure, and additional electrolyte was added. Figure 60 shows that the effect of the doubling of the $O_2$ was effective in reducing the $SO_2$ generation by 73%, with continuing decrease as time progressed, for a relatively constant cathodic potential of -6.2 Volts. The effect of the addition of electrolyte to the potential has already been established, but the $SO_2$ generation was again lowered, this time initially by about 50%. As the cathodic potential began to increase, the $SO_2$ generation also increased. This would suggest that the theory that the solidification of $SO_4^{-2}$ on the electrode surface over time might be partially responsible for inability of the electrolyte to internally utilize the $SO_2$; the decreasing surface area available for $O_2$ transport could force the equilibrium in Equation (67) to the right-hand side in a perpetuating cycle.

Upon breakdown, the relative color of the VK38 pellets in the channel showed a change in color only for the pellets nearest the exit, suggesting that any in-channel conversion of $SO_2$ to $SO_3$ was taking place primarily at the exit, at approximately 0.36 micromoles/min based on one pellet. However, the change due to the partial pressure of $O_2$ present was not known. It was therefore determined that a full-scale cell test should be implemented without the VK38 pellets in the flow channels.

The temperature of the cell was brought up slowly under pure $O_2$ on both the cathodic and anodic sides in the attempt to insure the full burnout and removal of the organics from the two ceramic and four electrolyte tapes. As the run continued, the wet seal was determined to be virtually perfect, having the ability to withstand large pressure gradients. Unfortunately, the mass flow measurements did not converge

throughout the experiment, suggesting the absorption or adsorption of the gas into the organic present. Organic was observed in the exit tubes, and was cleaned. This process was to no avail as the mass balances continued to be in error, and more organic material streamed out of the cell. Measurements should therefore be considered relative only to this cell, and not compared against previous data.

Data was evaluated at $P(O_2)$ of 0.03, 0.06, and 0.12 atm, at flowrates of 500cc/min to 545cc/min. Increases from 500cc/min were due to the addition of $O_2$. Figure 79 shows a limitation, probably due to mass transfer, on the cathode side, increasing with $O_2$ partial pressure, while the anode shows a decreasing limitation with increasing cathodic $O_2$ partial pressure. Evaluation of the data at low overpotential leads to the exchange current densities seen in Table XIV. These values are in agreement with earlier values (at 0.03 atm $O_2$, and 10wt% $V_2O_5$) seen in Table XIII, but the removal rates obtained are far from stoichiometric as seen in Figure 80. These results suggest slower overall kinetics with increasing $O_2$ partial pressure, indicating a trade-off between increased reoxidation of the $V^{4+}$ to $V^{5+}$ and overall reaction rate.

With the inability of the mass flows to balance, the error involved is substantial. On average, the mass balances were 50% in error. Examination of the rate of $SO_2$ production shows a definite decrease from a partial pressure of 0.06 atm to 0.12 atm, but, for this same cell, the initial partial pressure of 0.03 has a lower production rate in the high current region, despite a large slope in the low current region (see Figure 81). The error in the mass balances denies any qualitative analysis of the effects of the $O_2$ partial pressure on the cell. The exceedingly high cell polarizations seen in Figure 79 at high

current densities may come from the inability of the cell to remove $SO_3$ from the cathode stream, thus channeling the current into internal reactions. This inability of the cell to achieve lower $SO_2$ production may be due to organics present from the burnout, reducing the surface area available for mass transfer. In addition, the $SO_4^{-2}$ formation at the surface may further reduce the available surface area, and lead to further formation of $SO_2$ over time. The increasing polarization of the cell over time may explaining the conflicting $SO_2$ production at low partial pressures, as the initial runs were done at low partial pressures, without addition of electrolyte at any point during the run.

**Table XIII.** Exchange current densities.

| wt. % $V_2O_5$ | T, ° C | $i_o$, mA/cm$^2$ |
|---|---|---|
| 5% | 400 | 0.052 |
| 7% | 400 | 0.115 |
| 7% | 425 | 0.106 |
| 10% | 400 | 0.133 |
| 5%, Franke[2] | 400 | 0.033 |

**Table XIV:** Variation of exchange current densities with $O_2$ partial pressure.

| $P(O_2)$, atm | Exchange Current Density, $mA/cm^2$ |
|---|---|
| 0.03 | 0.135 |
| 0.06 | 0.082 |
| 0.12 | 0.050 |

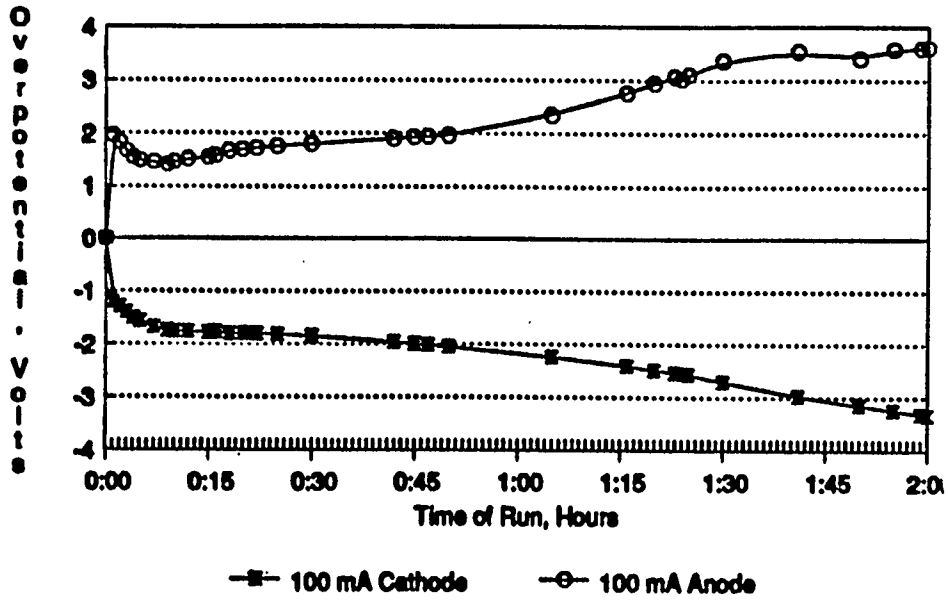


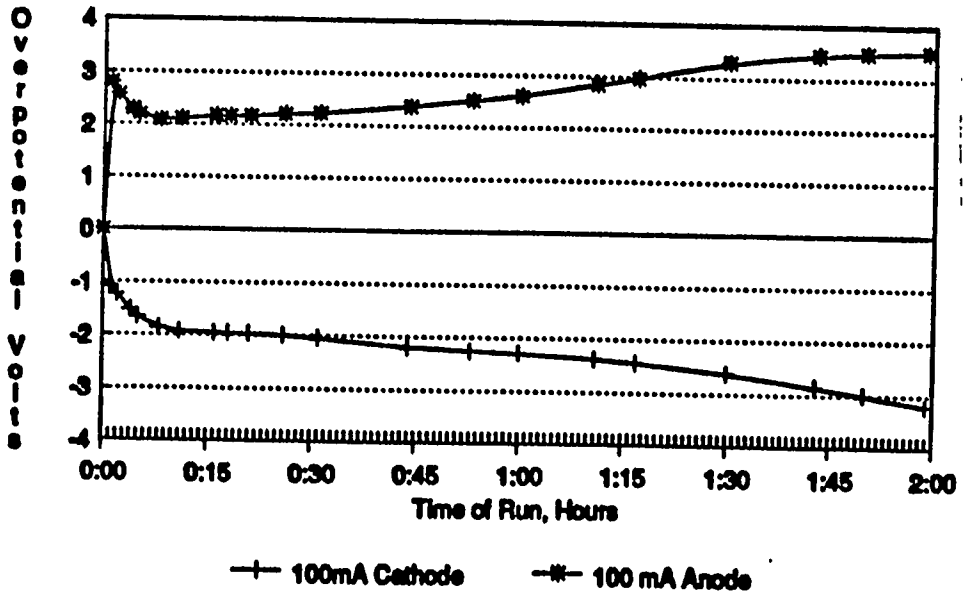


**Figure 61:** Comparison of overpotentials between runs utilizing identical components.

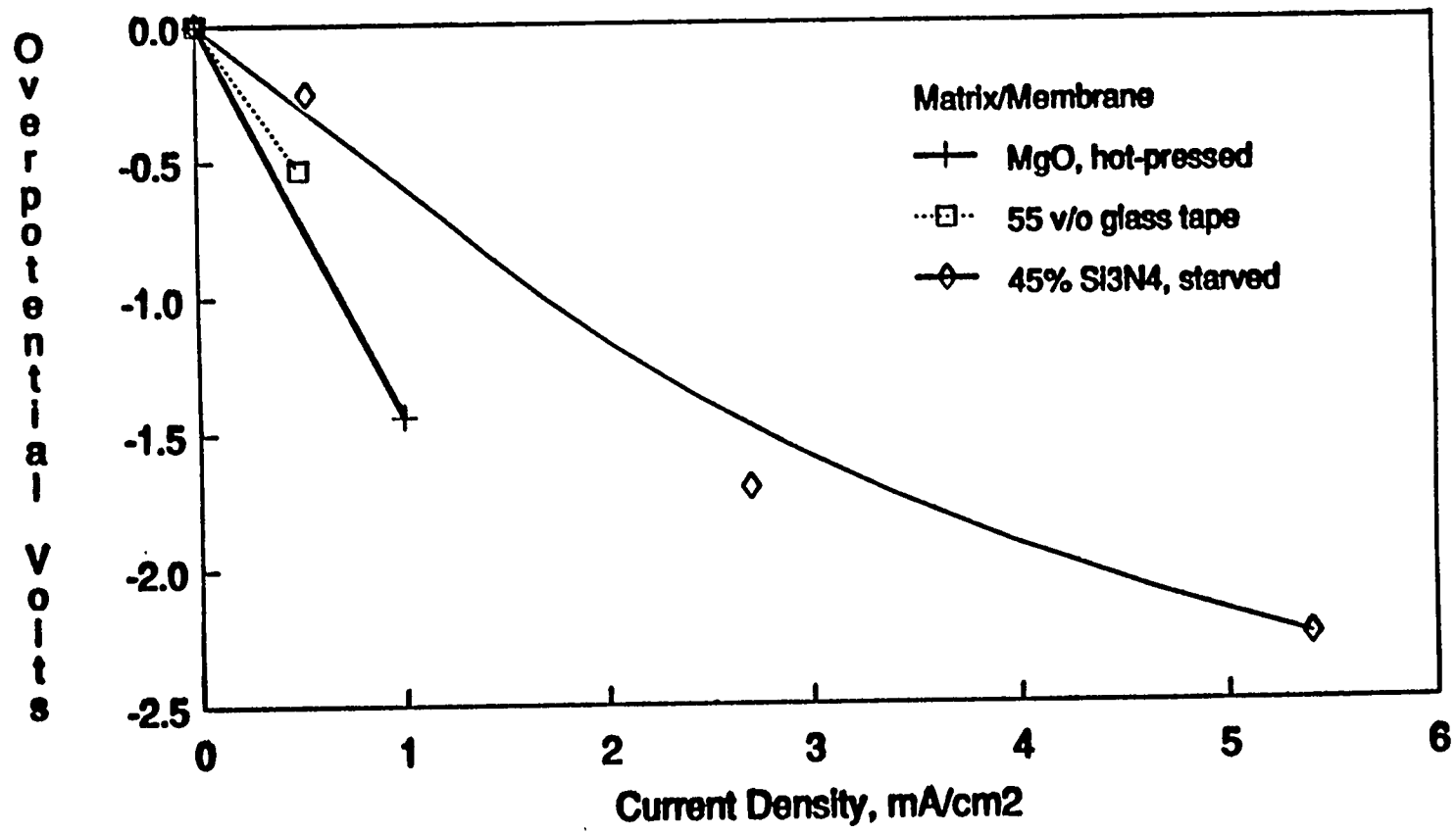


Figure 62: Overpotential versus applied current density comparison of the present and previous tests.

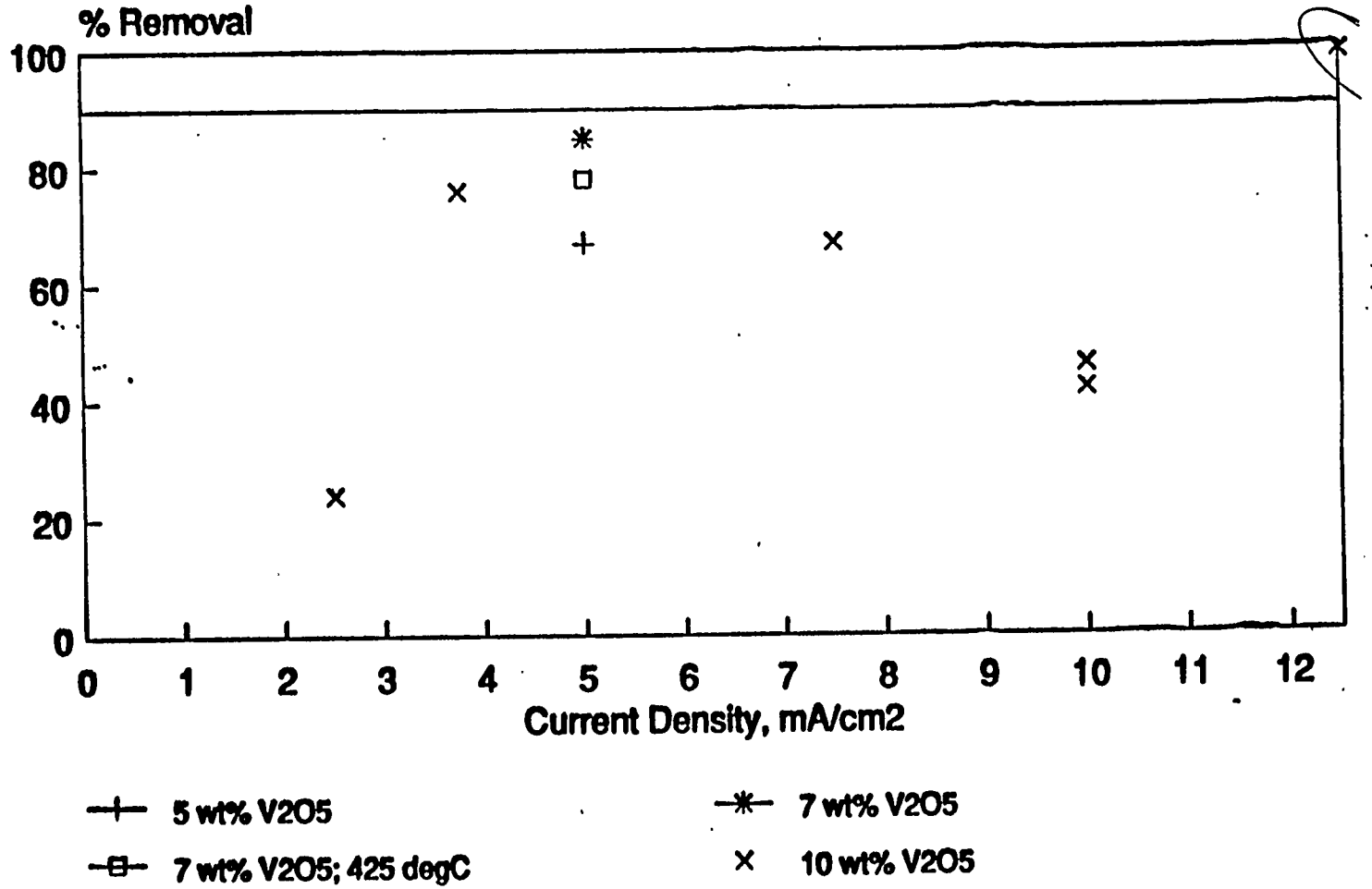


Figure 63. Cathodic removal of $SO_3$ after 10 minutes applied current. Flow of 0.3% $SO_2$, 3% $O_2$ in $N_2$ equal to that required for 90% removal at applied current.

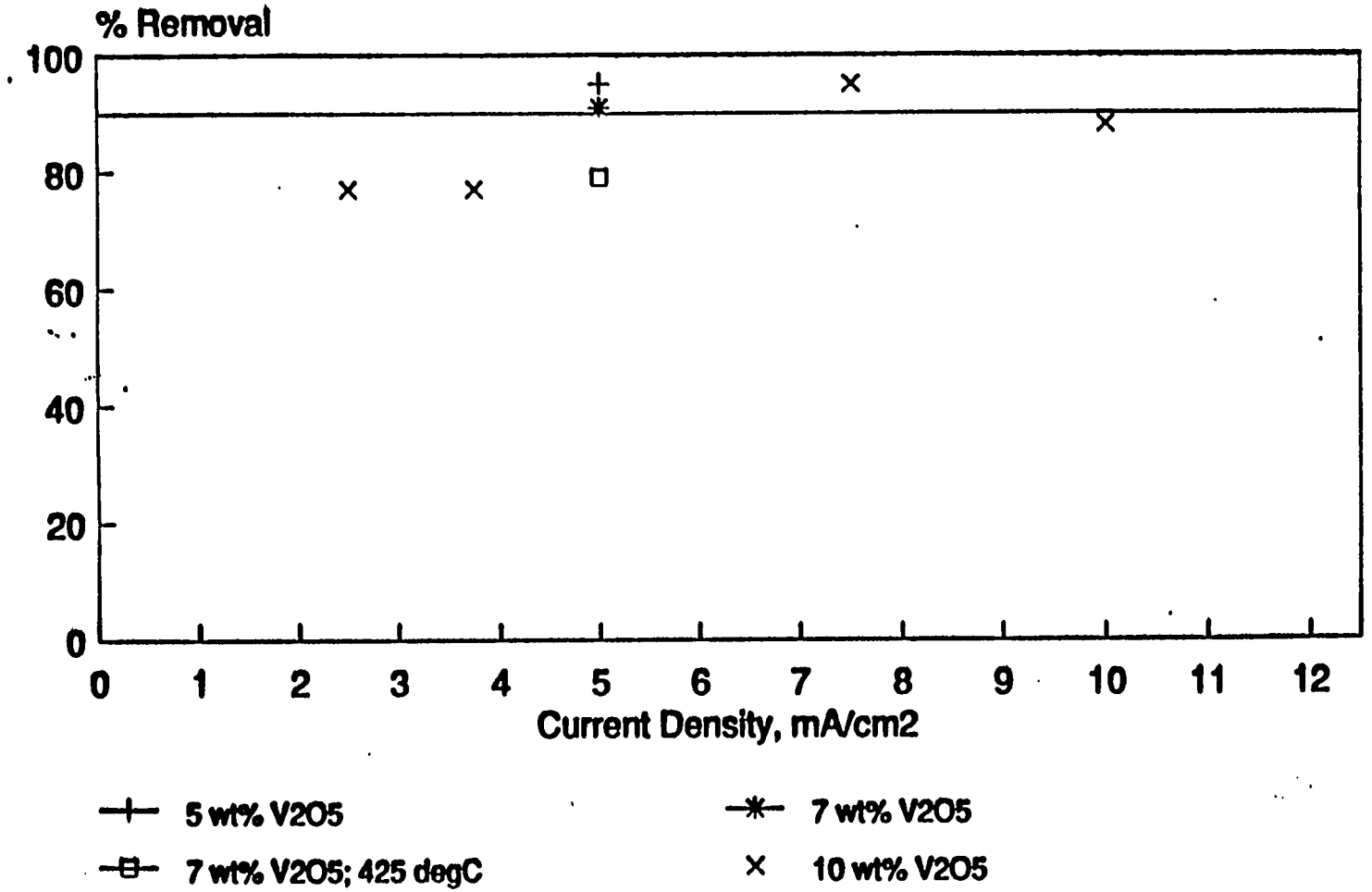


Figure 64. Cathodic removal of $SO_3$ after 60 minutes applied current. Flow of 0.3% $SO_2$, 3% $O_2$ in $N_2$ equal to that required for 90% removal at applied current.

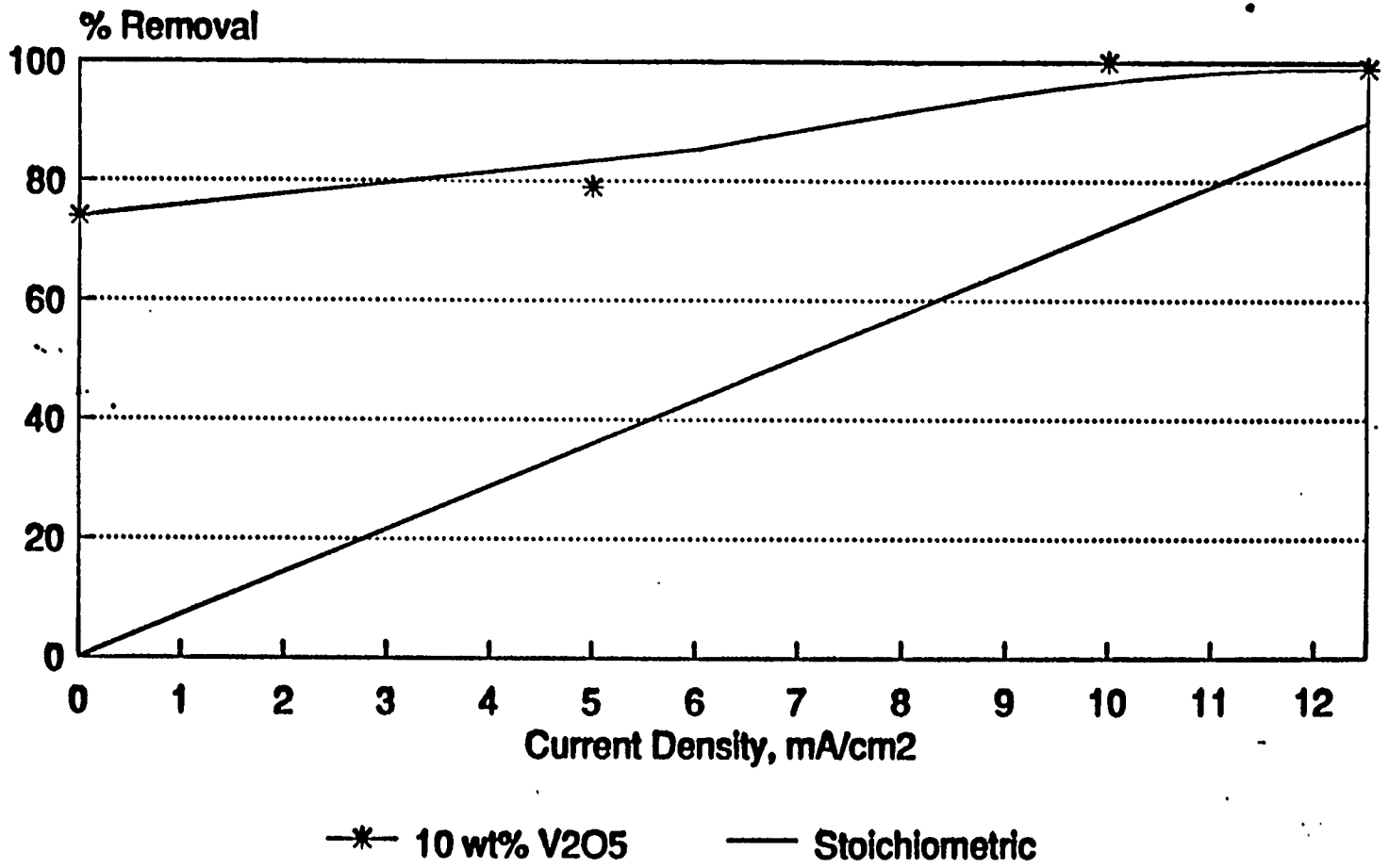


Figure 65. Cathodic removal of $SO_3$ with current. 690 cc/min of 0.31% $SO_2$, 3% $O_2$ in $N_2$ fed to cathode. All inlet $SO_2$ oxidized to $SO_3$. Line represents stoichiometric removal.

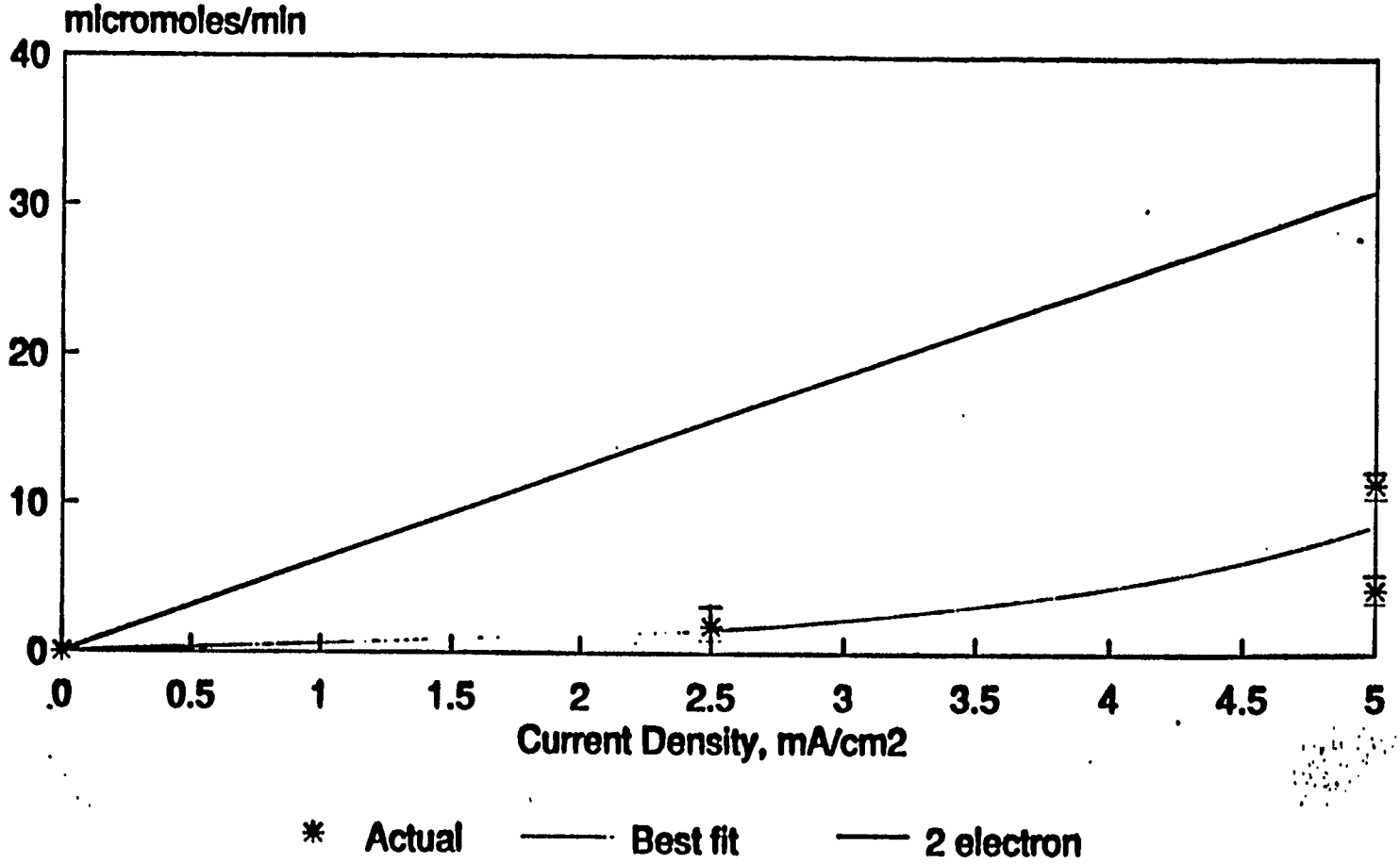


Figure 66. Cathodic $SO_2$ generation with applied current, with flow for 90% stoichiometric removal of inlet $SO_2$. 5 wt.% $V_2O_5$ in electrolyte.

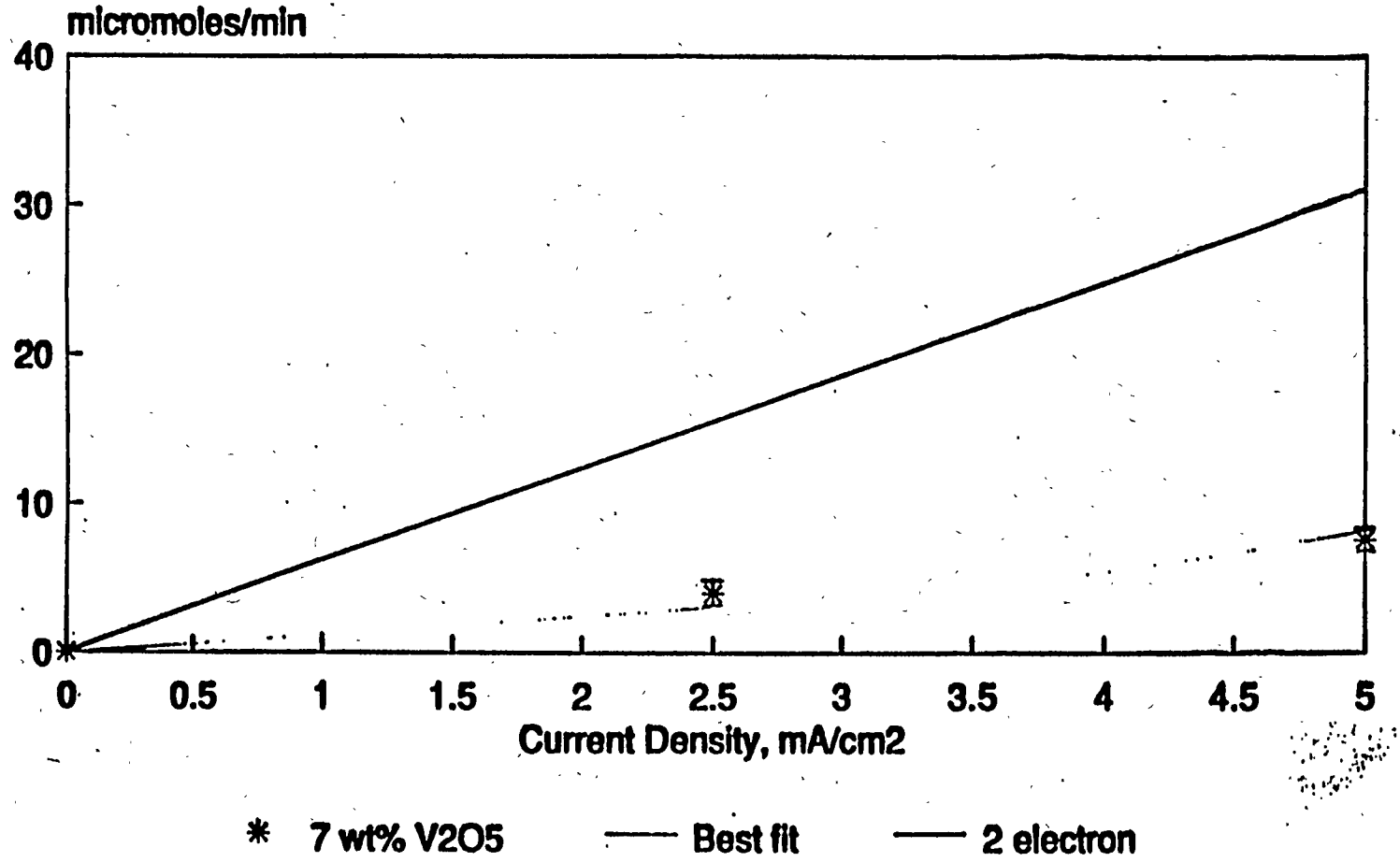




Figure 67. Cathodic $SO_2$ generation with applied current, with flow for 90% stoichiometric removal of inlet $SO_2$. 7 wt.% $V_2O_5$ in electrolyte.

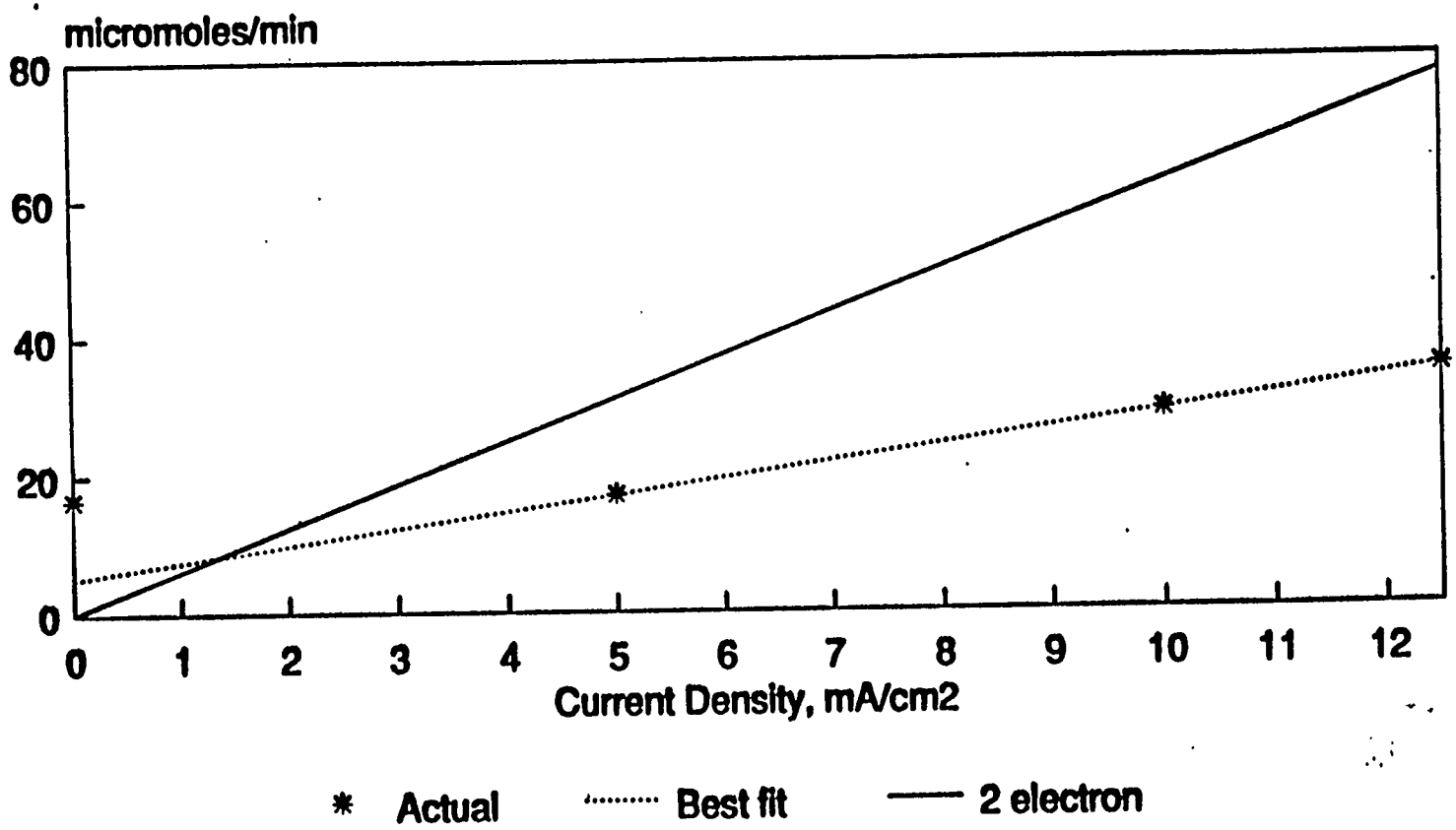


Figure 68. Cathodic $SO_2$ generation-Flow for 90% stoichiometric removal at 12.5 mA/cm$^2$. 10 wt.% $V_2O_5$ in electrolyte.

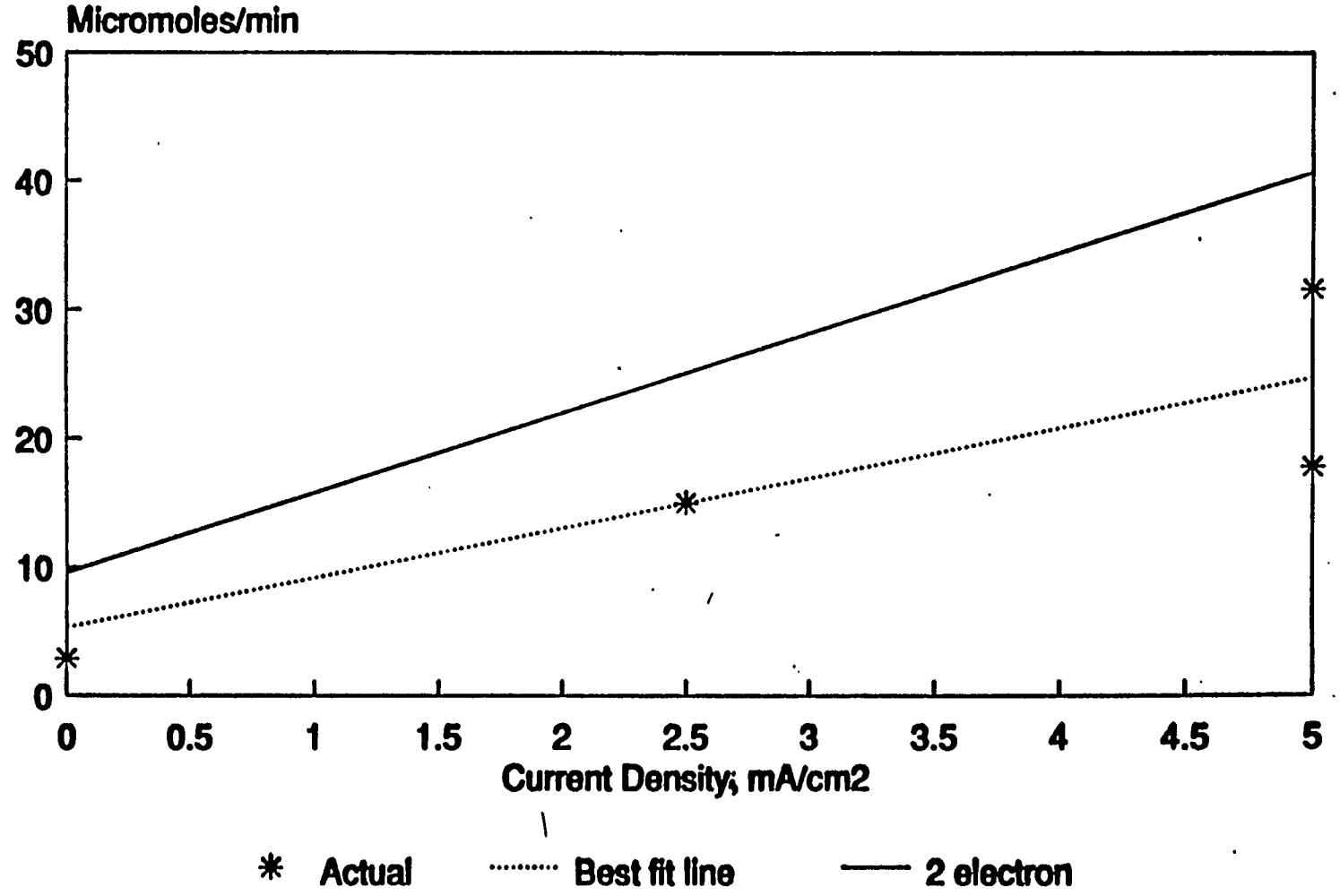


Figure 69. Anodic $SO_3$ generation, 5 wt.% $V_2O_5$ in electrolyte. Offset in calculated rates is due to oxidation of $SO_2$ fed to the anode side.

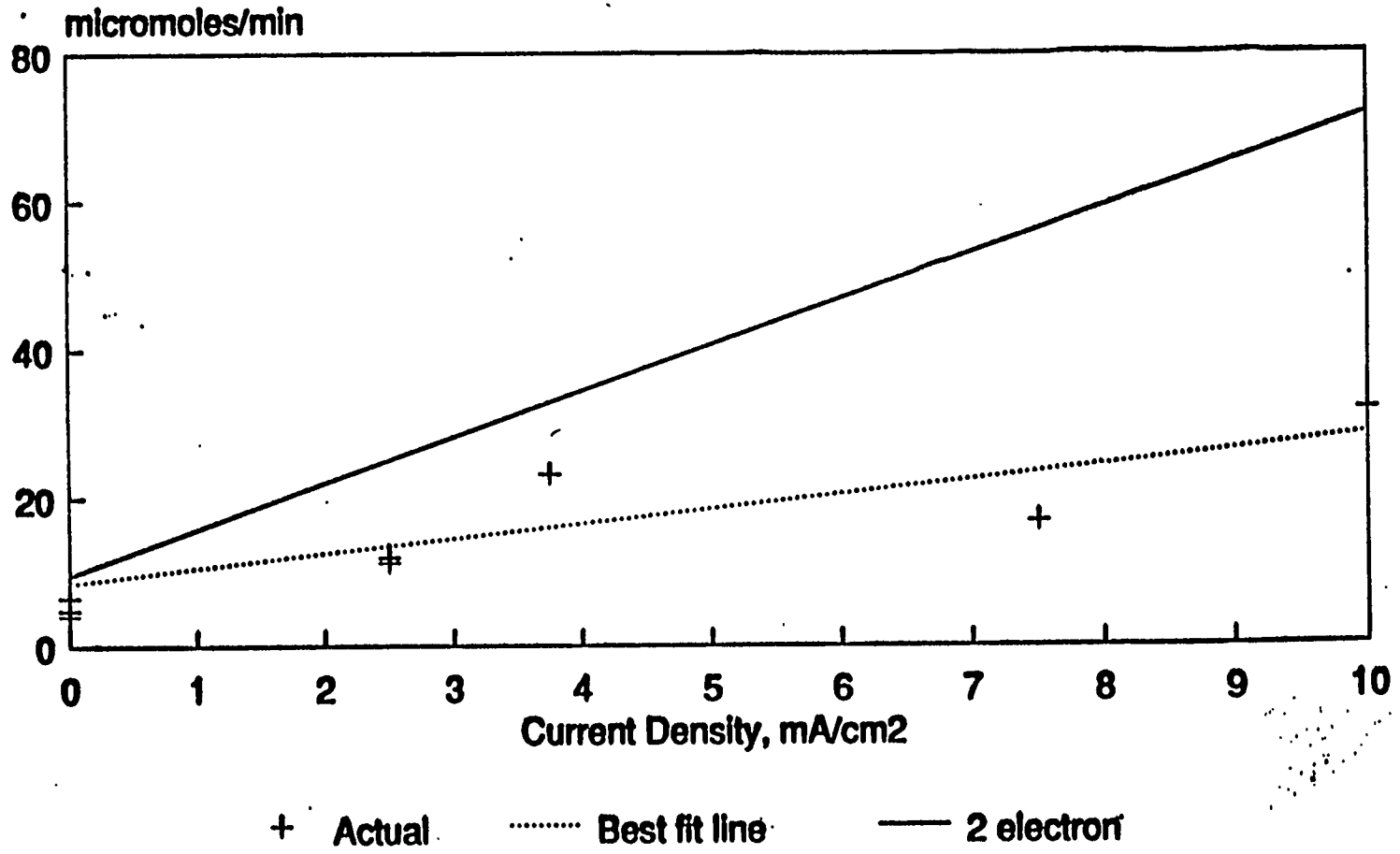


Figure 70. Anodic $SO_3$ generation, with 10 wt.% $V_2O_5$ in electrolyte. Offset in calculated rates is due to oxidation of $SO_2$ fed to the anode.

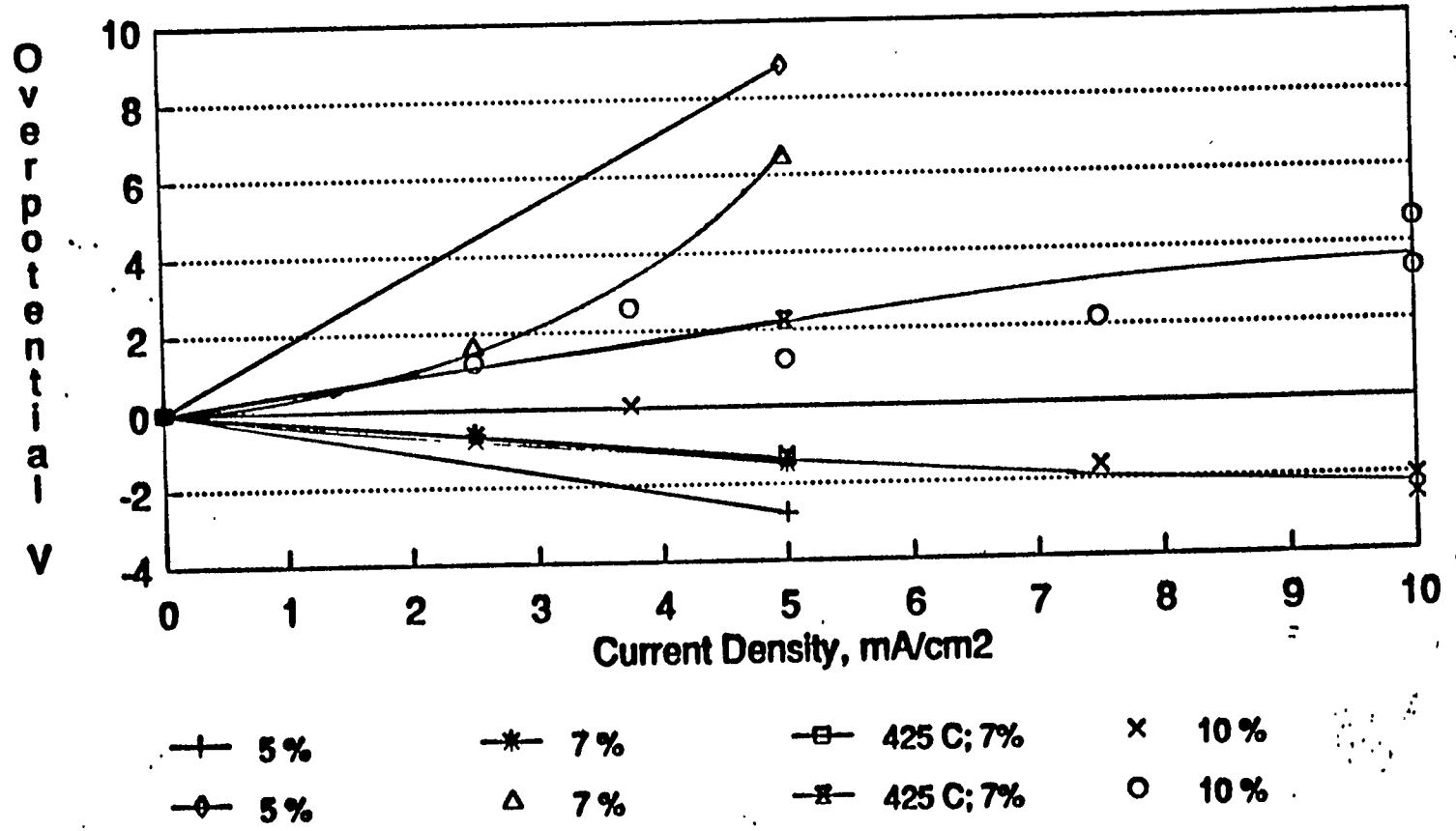


Figure 71. Polarization curves after 60 minutes of applied current.

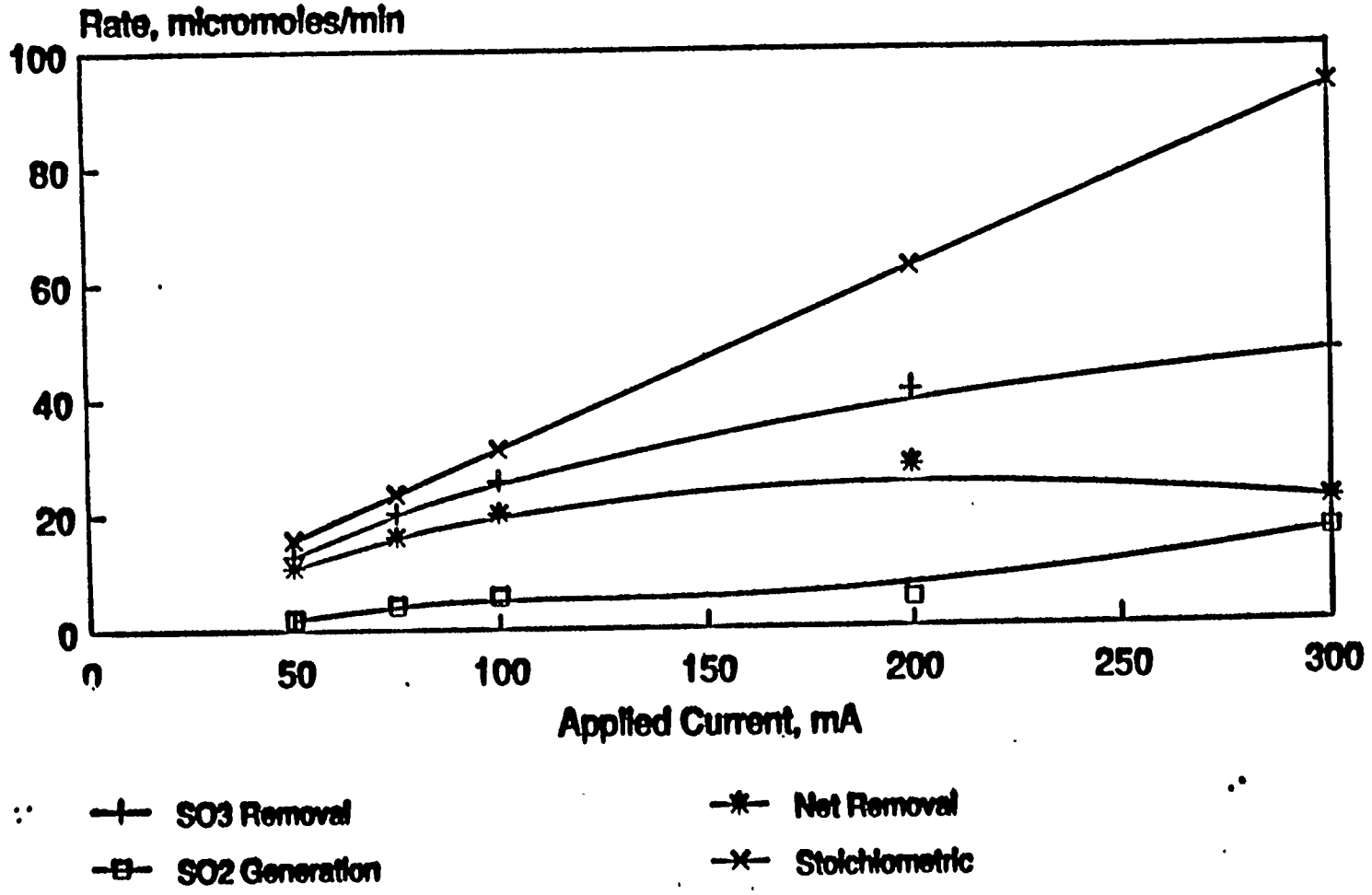


Figure 72:$SO_2$ generation and $SO_3$ removal as a function of applied current.

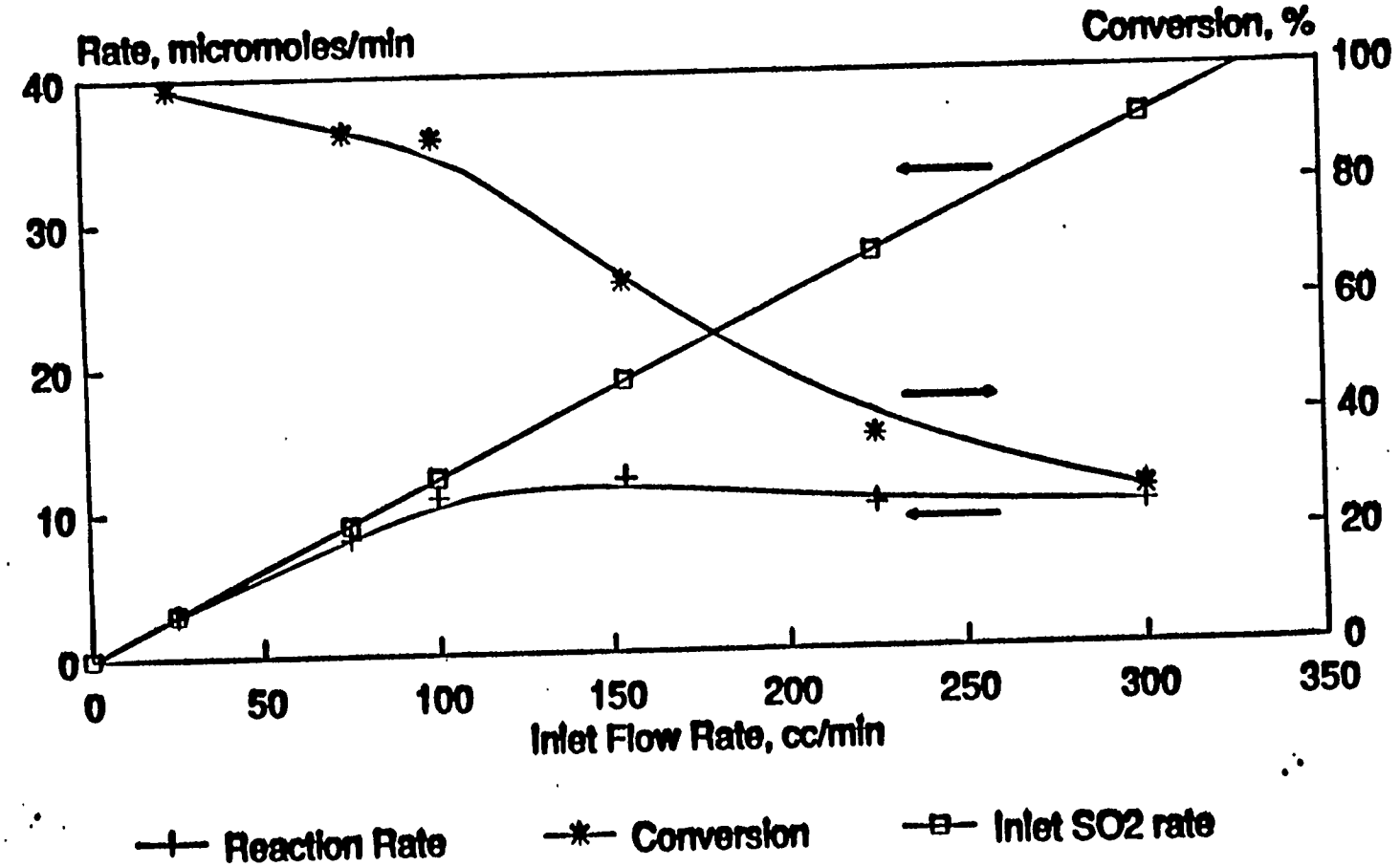


Figure 73. Rate and percent conversion of $SO_2$ over thin cylinders of VK38 catalyst at 400° C.

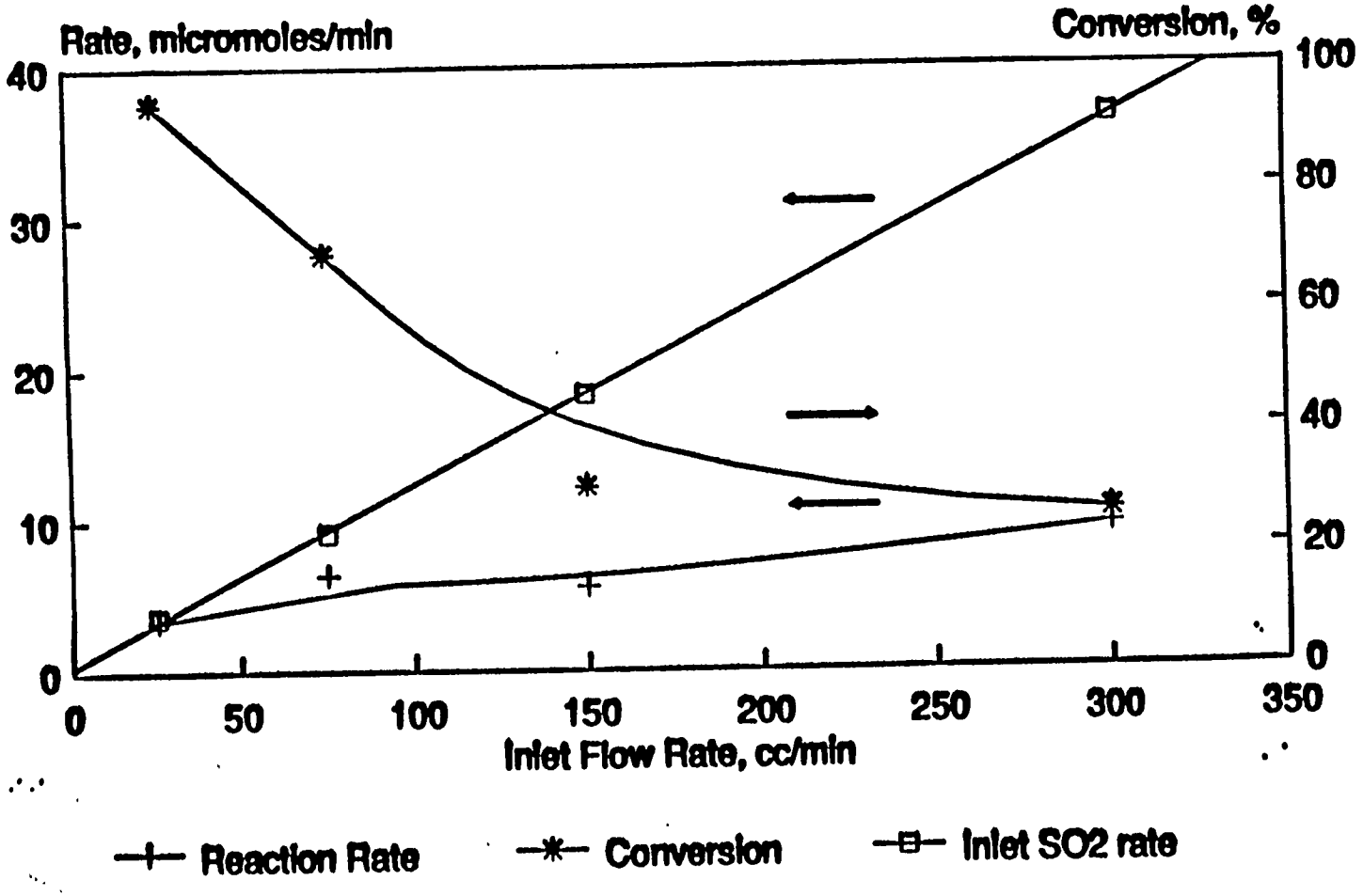


Figure 74. Rate and percent conversion of $SO_2$ over thin cylinders of VK38 catalyst at 375° C.

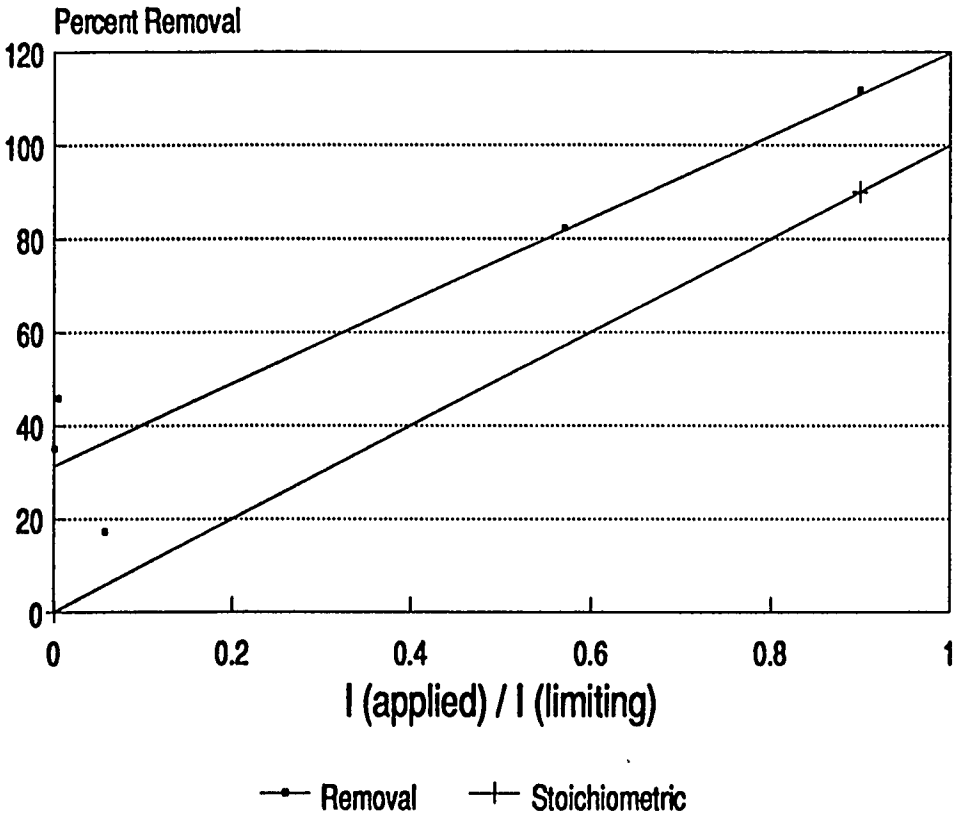


I (limiting)= 196 mA

**Figure 75:** The removal rate for the second run of the quarter.

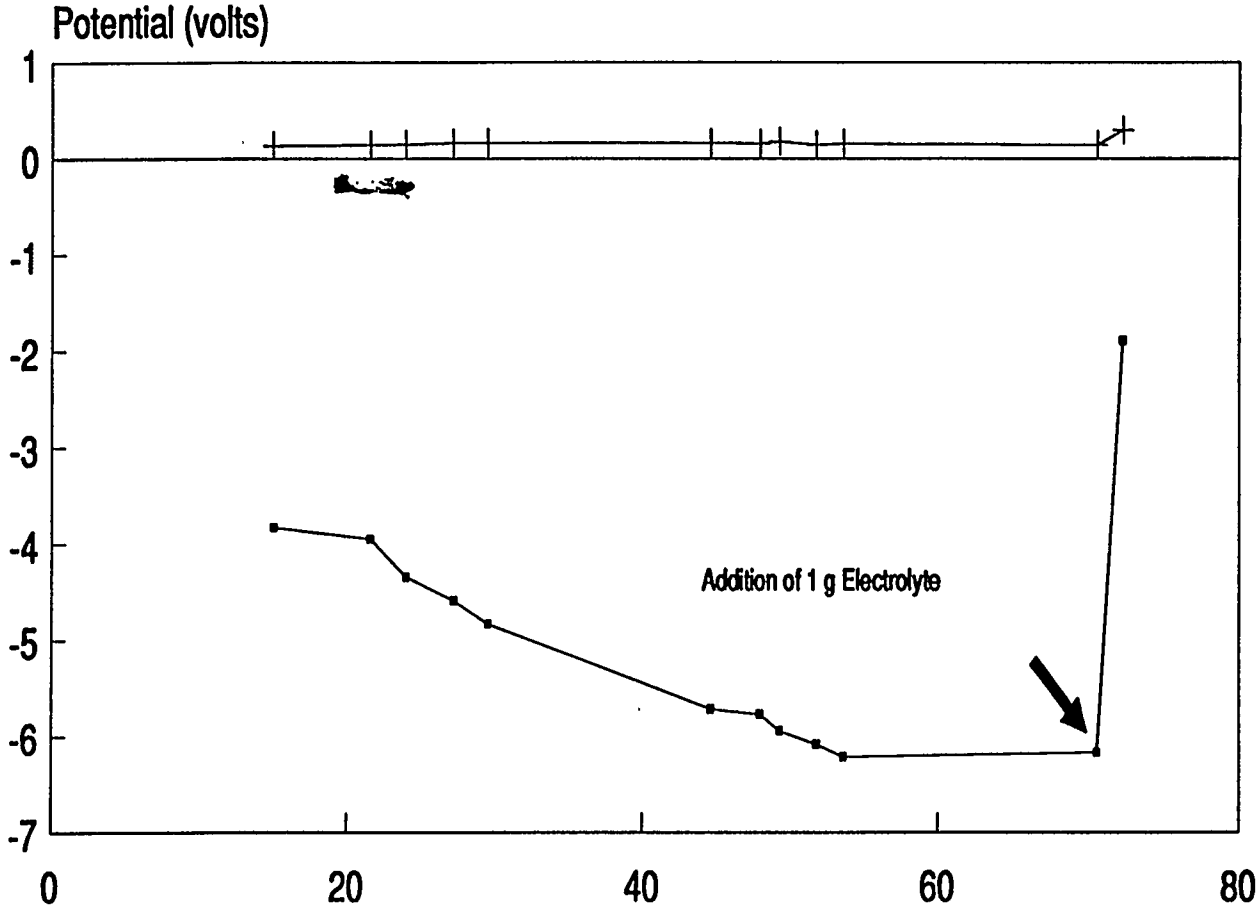


**Figure 76:** The general increase of the polarity of the cell dropped by 65% with the addition of 1g electrolyte.

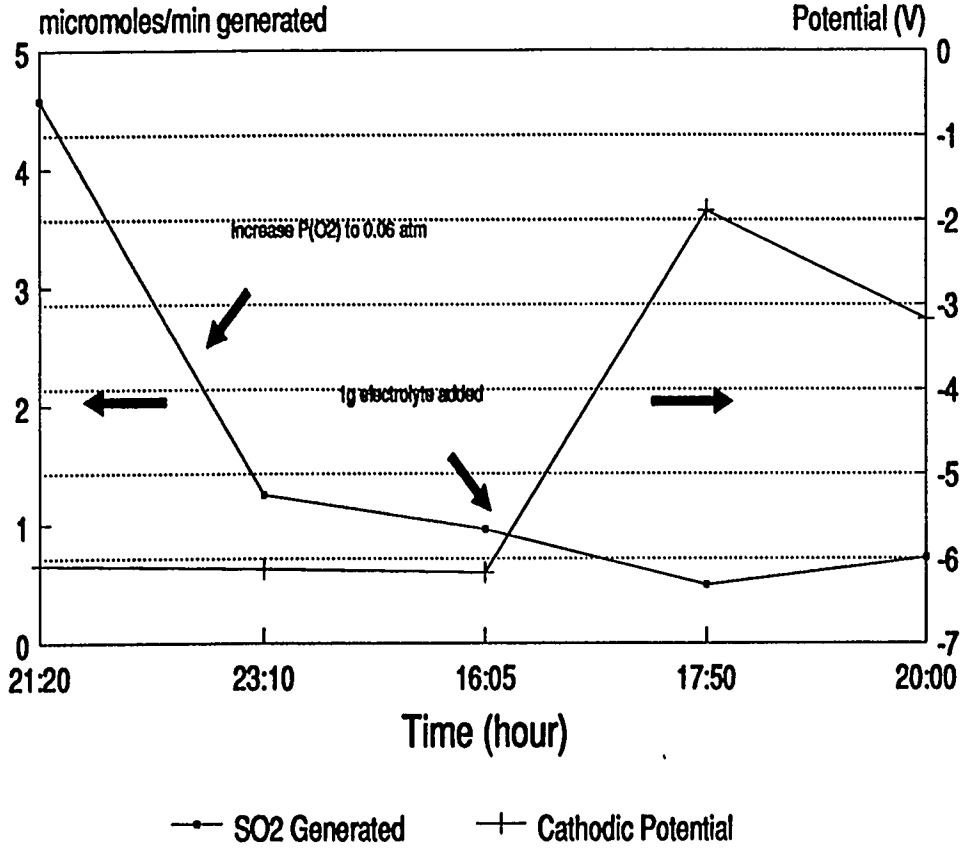


**Figure 77:** The change in both the cathodic potential and $SO_2$ generation with the increase in $P(O_2)$ and the addition of electrolyte.

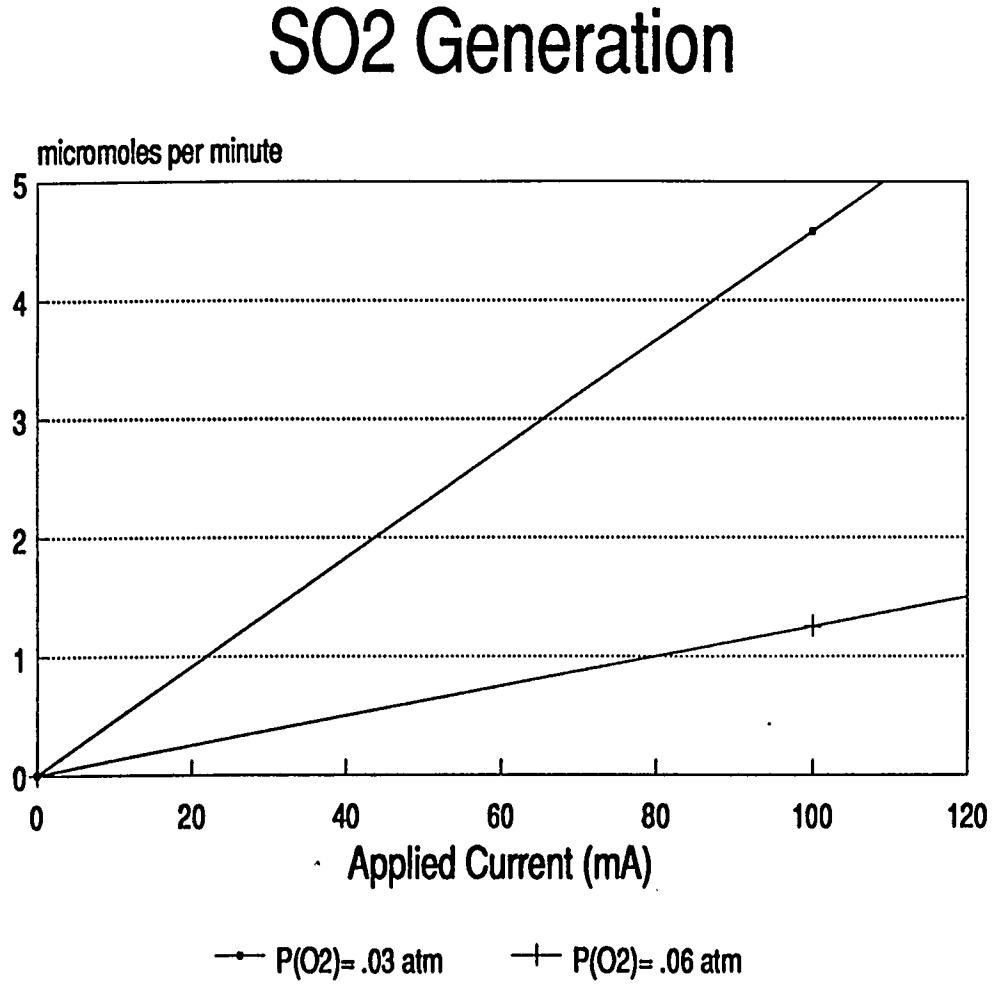


**Figure 78:** The extrapolated $SO_2$ generation for Run 2 with a change in the partial pressure of $O_2$ from .03 atm to .06 atm.

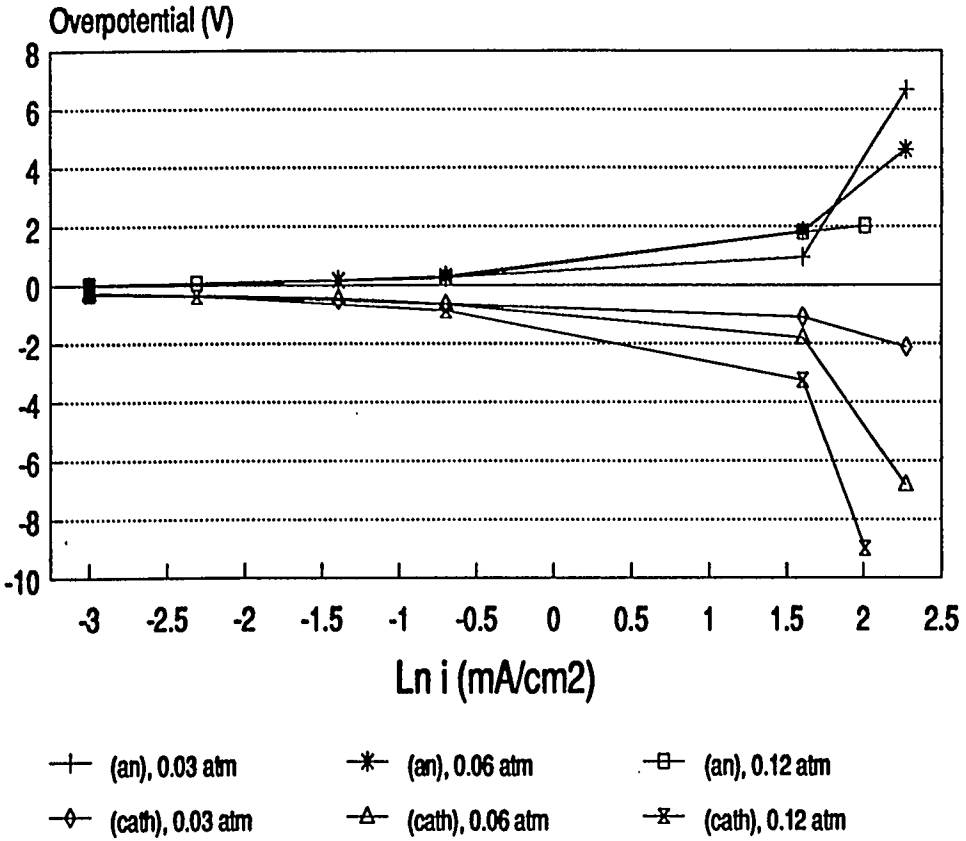


**Figure 79:** The variance of Overpotential (Volts) with ln i (mA/cm$^2$) at P($O_2$)=0.03 atm, 0.06 atm, 0.12 atm.

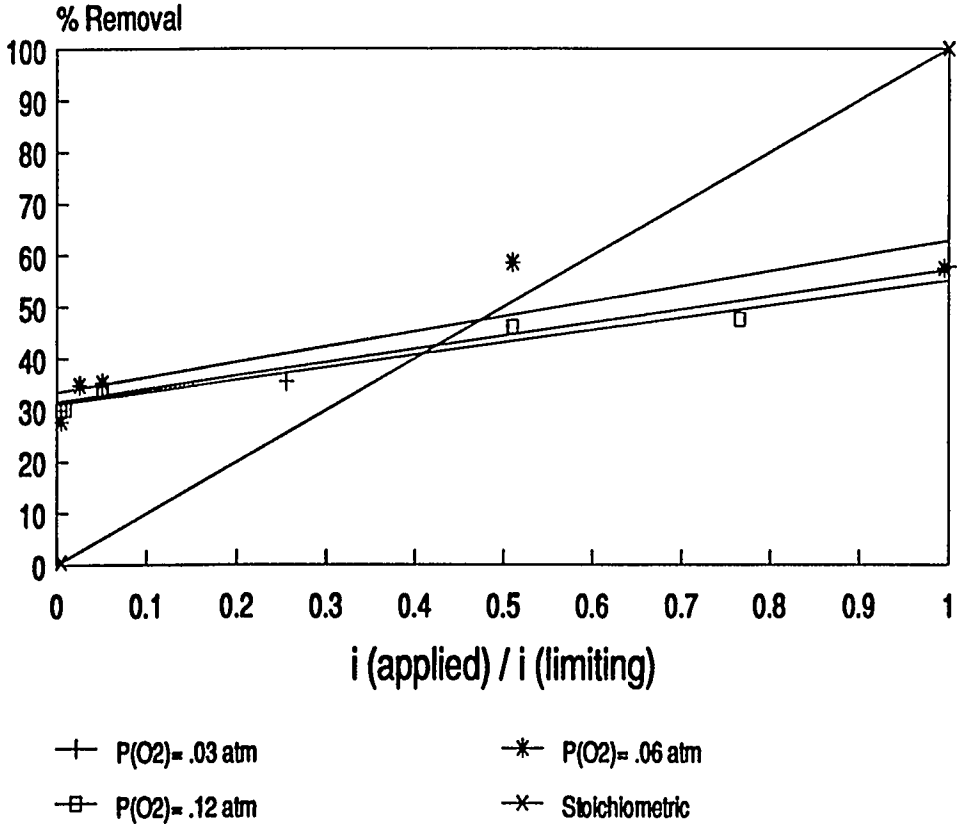


i(limiting)=19.8 mA/cm2

**Figure 80:** Removal rates based on cathode $SO_x$ for varying $O_2$ partial pressures.

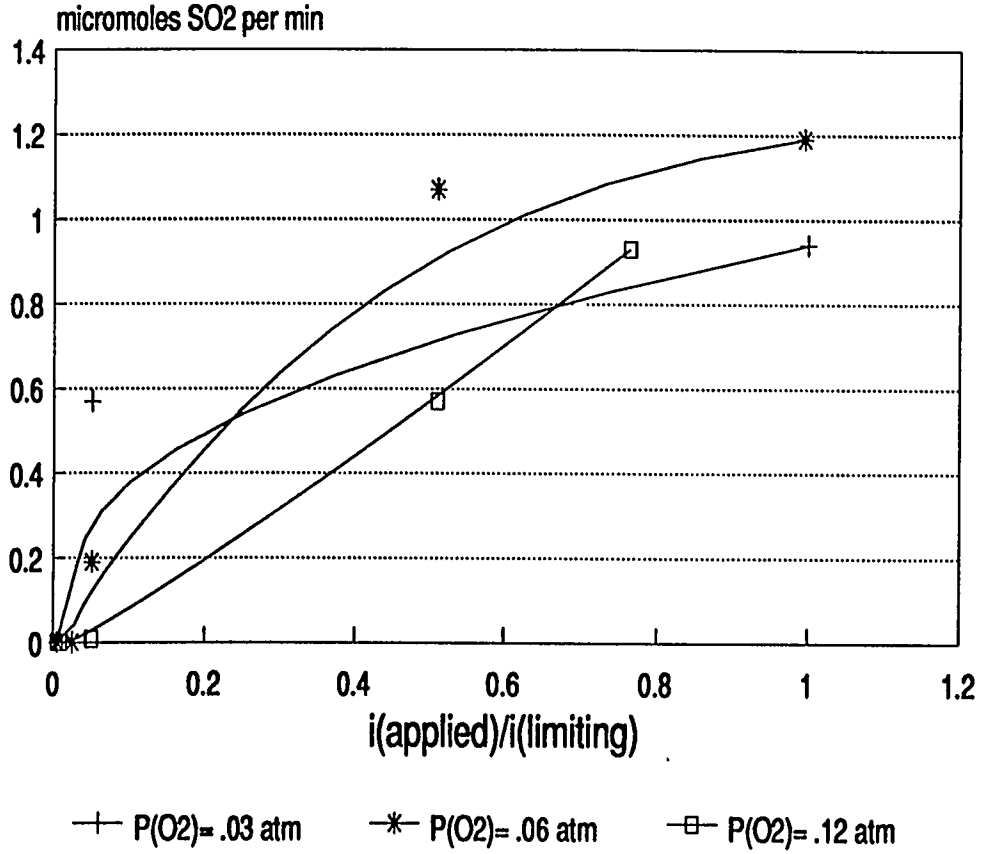


i (limiting)=19.8 mA/cm2

**Figure 81:** The production variance of $SO_2$ on the cathode side with various $P(O_2)$ for a constant flowrate.

## CONCLUSIONS

Strides have been made in material development for the $SO_2$ removal system. New lithiated NiO electrode have been developed, representing a great improvement over the previously used pervoskite electrodes. The electrodes have been shown to match the pore size specifications as well as exhibit chemical and electrochemical stability in the full cell system.

The greatest improvements have been seen in the development of the ceramic matrix. Of the vast materials tested, a good chemical and electrochemical match was found in the $Si_3N_4$ materials. In addition, the new tape casting method allowed the manufacture of extremely thin matrices with simple handling characteristics. The resulting matrix showed improvements over previously used matrices such as the MgO, as well as other materials tested.

Finally, the overall removal system has been shown to exhibit 90% removal at near 100% current efficiency, over a wide range of current densities. The one remaining problem, the evolution of $SO_2$ from the cathodic reactions, may be solved through the use of higher active area, necessitating the development of even electrodes with even smaller pore sizes. However, the results with the new materials prove extremely promising.

# CONCLUSION

The $H_2S$ cell has demonstrated over 90% removal capabilities in the 1000-100ppm, 100-10, and 10-1ppm $H_2S$ ranges. This excellent removal has been accompanied by economically feasible current efficiencies, with the highest current efficiencies (100%) in the 1000-100ppm $H_2S$ range. The lower current efficiencies experienced at polishing levels should still prove economically sound due to the low overall power requirement at those levels.

Yttria-stabilized densified zirconia membranes have shown a high degree of compatibility with the current system. Selective removal has been demonstrated in full cell testing as well as chemical and electrochemical stability in the basic environment. For polishing applications, lithiated Ni converted to NiO in-situ proved most useful for both cathode and anode materials, similar to the molten carbonate fuel cells. However, at $H_2S$ concentrations above 100ppm, a molten nickel sulfide state was shown to exist at the cathode, hindering high $H_2S$ removal efficiencies. This caused a shift toward Co cathodes proven to be stable and highly conductive in the carbonate environment.

The $SO_2$ removal cell consistently demonstrated 90% removal at near 100% current efficiency using a simulated flue gas stream of 3000ppm $SO_2$. $O_2$ was demonstrated as crucial to the removal process due to the regeneration of $V_2O_5$ from the $V^{4+}$ state.

After a number of materials had been tested, the tape-casting of $Si_3N_4$ was found to provide the most suitable membrane with respect to the chemical and electrochemical

stability in the highly acidic environment of the cell. In addition, the $Si_3N_4$ matrices was shown to provide lower polarizations than other candidate materials.

A new electrode, lithiated NiO was developed for use in the cell, and was found to resist the corrosive effect normally found with NiO in a sulfate-rich environment. Polarizations with these electrodes also led to their use in full cell system.

As this research period ended, focus was on increasing the electrode surface area available for reaction through the use of small electrode pore sizes. This method will also require the development of a ceramic matrix of smaller particle size.

# ENDNOTES


1. S. H. Langer and R. G. Haldeman, *J. Phys. Chem.*, **68** (1964) 962.

2. J. Winnick, R. D. Marshall, and F. H. Schubert, *I. E. C. Pr. Des.*, **13** (1974) 59.

3. H. S. Lim and J. Winnick, *J. Electrochem. Soc.*, **131** (1984) 562.

4. D. Weaver and J. Winnick, *J. Electrochem. Soc.*, **134** (1987) 2451.

5. S. Alexander and J. Winnick, 6th *Symp. Sep'n Sci. and Tech.*, in press.

6. K. A. White and J. Winnick, *Electrochem. Acta*, **30** (1985) 511.

7. E. K. Banks and J. Winnick, *J. Appl. Electrochem.*, **16** (1986) 583.

8. D. Weaver, Ph. D. Thesis, Georgia Institute of Technology, 1988.

9. Austin, I.G., and Mott, N.E., Adv. Phys., 18, 41 (1969).

10. Kingery, W.D., Brown, H.K., Uhlmann, C.R., Introduction to Ceramics, 2nd. ed., Wiley, New York, 1976.

11. Ellingham, J.T., *J. Soc. Chem. Ind.*, **63**, 125, (1944).

12. Weaver, D., Electrochemical Removal of $H_2S$ from Multicomponent Gas Streams, Georgia Institute of Technology PhD Dissertation, 1988.

13. Barin, I., and Knacke, O., Thermochemical Properties of Inorganic Substances, Springer-Verlag, Berlin, (1973).

14. Barin, I., and Knacke, O., Thermochemical Properties of Inorganic Substances - Supplement, Springer-Verlag, Berlin, (1977).

15. Preto, S.K., Tomzcuk, Z., et. al., *J. Electrochem. Soc.*, **130**, (1983).

16. Ingram,M.D., and Janz, G.J., *Electrochemica Acta*, **10**, (1965).

17. Babcock, K., and Winnick, J., *J. Chem. E. Data*, **33**, 1988.

18. Iacovangelo, C., and Karas, B., *J. ELectrochem. Soc.*, **133**, 1986.

19. Hamling, B., and Lattimer, R., *Advanced Materials and Processes*, June, 1986.

20.Flood, H.; Förland, T., *Acta. Chemica. Scandinavica*, **1** (1947), 781-789.

21. Flood, H.; Boyle, C., *Zeitschrift für Elektrochemie*, **66** (1962), 184.

22. Boreskov, G. K., *et. al.*, *J. Gen. Chem. USSR*, **24** (1954), 21.

23. Fang, W. C.; Rapp, R. A., *J. Electrochem. Soc.*, **130** (1983), 2335.

24. Park, C. O.; Rapp, R. A., *J. Electrochem. Soc.*, **133** (1986), 1636.

25. Shores, D. A.; Fang, W. C., *J. Electrochem. Soc.*, **128** (1981), 346.

26. Franke, M. D., Electrochemical Flue Gas Clean-Up, Ph.D. Thesis, Georgia Institute of Technology, 1988.

27. Scott, K. D.,Electrochemical Flue Gas Desulfurization, Ph.D. Thesis, Georgia Institute of Technology, 1985.

28. Townley, D.; Winnick, J., *I.&E.C. Proc. Desgn. & Develop.*, **20** (1981), 435.

29. Salzano, F. J.;Newman, L., *J. Electrochem. Soc.*, **119** (1972), 1273.

30. Flood, H.; Kleppa, O. J., *J. Am. Chem. Soc.*, **69** (1947), 998.

31. Karydis, D. A., *et. al.*,"Extended Abstracts," *J. Electrochem. Soc.*, **93-1** (1993), 2017.

32. Karydis, D., *et. al.*, "Extended Abstracts," *J. Electrochem. Soc.*, **93-1** (1993), 2027.

33. Hodgman, Charles D. et. al., Eds., Handbook of Chemistry and Physics, 42nd Edition, 1960-1961, Chemical Rubber Publishing Company, Cleveland, Ohio, 1960.

34. Prausnitz, J.M., Lichtenthaler, R.N.,deAzevedo, E.G.,Molecular Thermodynamics of Fluid-Phase Equilibria, Prentice-Hall, New Jersey, 1986.

35. Lovering, Gale et. al., Molten Salt Techniques vol. 1, 1983.

36. Jaeger, F.M., "Z. Anorg. Chem.," 101, 1 (1917).

37.Burrows, B.W., and Hills G.J., *Electrochim. Acta.* **15**(1970), 445.

38.Risbud, S.H., Zangvil, A.,*J. Matl. Sci.*, **18**(1983), 998.

39. D.N. Hill, Professor, Ceramic Engineering, Georgia Institute of Technology, personal communication.

40. Chin G.Y., Advances in Powder Technology, American Society for Metals, 1982, p.293.

41. Mark Wesselman, Electro Scientific Industries, personal communication.

42. Scott, K. D., Fannon, T. and Winnick, J., *J. Electrochem. Soc.*, **135**, 573, 1988.

43. Franke, M. and Winnick, J., *I&EC Research*, **28**, 1352, 1989.

44. Holroyd, F. P. B. and Kenney, C. N., *Chem. Eng. Sci.*, **26**, 1963, 1971.

45. Holroyd, F. P. B. and Kenney, C. N., *Chem. Eng. Sci.*, **26**, 1971, 1971.

46. Mars, P. and Maessen, J. G. H., *J. Catalysis*, **10**, 2, 1968.

47. Franke, M. and Winnick, J., ***J. Electroanalytical Chemistry*, 238**, 163, 1987.

48. McHenry, Dennis John, Development of an Electrochemical Membrane Process fir Removal of $SO_x/NO_x$ from Flue Gas, Ph.D. Thesis, Georgia Institute of Technology, 1992.